Supporting Information

The comparative studies on the magnetic relaxation behaviour of the axially-elongated pentagonal-bipyramidal dysprosium and erbium ions in similar one-dimensional chain structures

Fei Wang,‡[a] Hui-Wen Gong,‡[a] Yan Zhang,[a] An-Qi Xue,[a] Wen-Hua Zhu,*[a] Yi-Quan Zhang,*[c] Zhen-Na Huang,[d] Hao-Ling Sun,*[d] Bei Liu,[a] Yue-Yi Fang[a] and Song Gao*[b]

[a]Collaborative Innovation Center for Advanced Organic Chemical Materials Co-constructed by the Province and Ministry, Ministry-of-Education Key Laboratory for the Synthesis and Application of Organic Functional Molecules, College of Chemistry and Chemical Engineering, Hubei University, Wuhan 430062, P. R. China.

[b]Beijing National Laboratory for Molecular Sciences, State Key Laboratory of Rare Earth Materials Chemistry and Applications, College of Chemistry and Molecular Engineering, Peking University, No. 5 Yiheyuan Road, Beijing 100871, P. R. China.

[c]Jiangsu Key Lab for NSLSCS, School of Physical Science and Technology, Nanjing Normal University, Nanjing, Jiangsu 210023, P. R. China.

[d]Department of Chemistry and Beijing Key Laboratory of Energy Conversion and Storage Materials, Beijing Normal University, Beijing 100875, P. R. China.

Email: zhuwenhua@hubu.edu.cn; Email: gaosong@pku.edu.cn;
Email: zhangyiquan@njnu.edu.cn; Email: haolingsun@bnu.edu.cn.

1. Experimental Section

Materials and physical techniques

Unless otherwise stated, all chemicals and solvents were of analytical reagent grade and used as purchased without further purification. All reactions were carried out under aerobic conditions. Elemental analyses of C, H and N were carried out on a Vario Micro Cube elemental analyzer (Elementar Aanlysensysteme GmbH, Germany). IR spectra (4000–400 cm^{-1}) on powered samples were recorded on a Perkin Elmer Spectrum one spectrophotometer using KBr pellets. Powder X-ray diffraction (PXRD) data for the as-prepared samples were collected on a D8 ADVANCE (Bruker AXS, Germany) diffractometer at room temperature using Cu-Kα radiation.

X-ray crystallography

Determination of the unit cell and data collection for complexes **1**−**5** at 298 K were performed on a Bruker Smart APEX II CCD area detector diffractometer with graphite-monochromated Mo K_α radiation (λ = 0.71073 Å). All of the diffraction data were collected at room temperature and corrected for Lorentz and polarization effects. Adsorption corrections were applied by SADABS method.[1] Using Olex2,[2] the structures were solved by direct methods of SHELXS-97 program and refined by the full-matrix least-squares techniques based on F^2 using SHELXL-2013 program.[3a,b] All of the ordered non-hydrogen atoms were refined with anisotropic thermal parameters. Hydrogen atoms of the coordinated and lattice H_2O molecules were located by difference Fourier map and refined isotropically with constrains for the ideal geometry of H_2O molecules with an O−H distance of 0.96 Å and an H−O−H angle of 105°. Organic hydrogen atoms were introduced on calculated positions and refined with isotropic thermal parameters and a fixed geometry riding on their parent atoms.[3c,d] The crystal data and structural refinement details of **1**−**5** are respectively summarized in Table 1. The selected bond lengths and angles of **1**−**5** are listed in Tables S1−S9 in the ESI. CCDC 2072135, 2072136, 2072141, 2072147 and 2072150.

Magnetic measurement

Static magnetic measurements including temperature-dependent magnetic susceptibility in the range of 2−300 K, and field-dependent magnetization of **1**−**5** were carried out on a Quantum Design MPMS-XL5 SQUID magnetometer. AC susceptibilities of **1**−**5** (100−10000 Hz) were measured using a Quantum Design PPMS magnetometer. All of the magnetic measurements were performed on polycrystalline samples tightly packed with grease and sealed with film to avoid the anisotropic orientation. Diamagnetic corrections were made with Pascal's constants for all the constituent atoms.[4]

2. Structural Data and Diagram

Table S1 Selected bond lengths (Å) and angles (°) for **1**

Y(1)–O(1)	2.281(8)	Y(1)–O(2)	2.292(9)
Y(1)–O(3)	2.308(8)	Y(1)–O(4)	2.270(9)
Y(1)–O(5)	2.262(8)	Y(1)–N(1)	2.337(9)
Y(1)–N(2)#1	2.364(11)		
Fe(1)–C(1)	1.910(13)	Fe(1)–C(2)	1.894(11)
Fe(1)–C(3)	1.929(18)	Fe(1)–C(4)	1.945(14)
Fe(1)–C(5)	1.953(15)	Fe(1)–C(6)	1.932(15)
O(1)–Y(1)–O(2)	71.9(3)	O(1)–Y(1)–O(3)	137.9(3)
O(1)–Y(1)–O(4)	143.4(3)	O(1)–Y(1)–O(5)	72.1(3)
O(2)–Y(1)–O(3)	71.6(3)	O(2)–Y(1)–O(4)	144.7(3)
O(2)–Y(1)–O(5)	138.9(3)	O(3)–Y(1)–O(4)	75.1(3)
O(3)–Y(1)–O(5)	148.7(3)	O(4)–Y(1)–O(5)	73.7(3)
O(1)–Y(1)–N(1)	83.4(3)	O(1)–Y(1)–N(2)#1	102.4(3)
O(2)–Y(1)–N(1)	100.6(3)	O(2)–Y(1)–N(2)#1	84.0(4)
O(3)–Y(1)–N(1)	83.5(3)	O(3)–Y(1)–N(2)#1	93.9(3)
O(4)–Y(1)–N(1)	86.7(3)	O(4)–Y(1)–N(2)#1	86.9(4)
O(5)–Y(1)–N(1)	94.3(3)	O(5)–Y(1)–N(2)#1	84.8(4)
N(1)–Y(1)–N(2)#1	173.6(5)		
C(1)–Fe(1)–C(2)	178.7(6)	C(1)–Fe(1)–C(3)	89.7(5)
C(1)–Fe(1)–C(4)	89.6(5)	C(1)–Fe(1)–C(5)	89.4(5)
C(1)–Fe(1)–C(6)	90.8(5)	C(2)–Fe(1)–C(3)	89.0(5)
C(2)–Fe(1)–C(4)	89.9(5)	C(2)–Fe(1)–C(5)	91.9(5)
C(2)–Fe(1)–C(6)	89.6(5)	C(3)–Fe(1)–C(4)	88.8(6)
C(3)–Fe(1)–C(5)	179.1(6)	C(3)–Fe(1)–C(6)	88.6(6)
C(4)–Fe(1)–C(5)	91.1(6)	C(4)–Fe(1)–C(6)	177.3(6)
C(5)–Fe(1)–C(6)	91.6(6)		
N(1)–C(1)–Fe(1)	178.9(12)	N(2)–C(2)–Fe(1)	178.3(12)
C(1)–N(1)–Y(1)	175.9(10)	C(2)–N(2)–Y(1)#2	178.7(12)

Symmetry codes： #1 x+1/2,y+1/2,z, #2 x–1/2,y–1/2,z.

Table S2 Hydrogen bonding geometry for **1**: lengths (Å) and angles (°)

D–H···A	d(D–H)	d(H···A)	d(D···A)	<(DHA)
O(7)–H(7A)···N(4)	0.96(3)	1.99(7)	2.898(16)	158(15)
O(7)–H(7B)···O(6)#3	0.95(3)	1.94(10)	2.790(17)	147(17)
O(8)–H(8A)···N(6)	0.96(3)	2.08(14)	2.813(17)	132(15)
O(9)–H(9B)···N(5)	0.96(3)	2.14(7)	3.031(17)	154(12)

Symmetry codes： #1 x+1/2,y+1/2,z, #2 x–1/2,y–1/2,z, #3 x–1/2,y+1/2,z.

Table S3 Selected bond lengths (Å) and angles (°) for **2**

Dy(1)–O(1)	2.297(4)	Dy(1)–O(2)	2.315(4)
Dy(1)–O(3)	2.298(4)	Dy(1)–O(4)	2.294(4)
Dy(1)–O(5)	2.340(4)	Dy(1)–N(1)	2.382(5)
Dy(1)–N(4)	2.385(5)		
Fe(1)–C(1)	1.910(6)	Fe(1)–C(2)	1.953(7)
Fe(1)–C(3)	1.951(8)	Fe(2)–C(4)	1.910(6)
Fe(2)–C(5)	1.957(7)	Fe(2)–C(6)	1.959(8)
O(1)–Dy(1)–O(2)	71.78(15)	O(1)–Dy(1)–O(3)	139.42(14)
O(1)–Dy(1)–O(4)	148.10(15)	O(1)–Dy(1)–O(5)	74.29(15)
O(2)–Dy(1)–O(3)	70.37(15)	O(2)–Dy(1)–O(4)	140.09(15)
O(2)–Dy(1)–O(5)	143.14(16)	O(3)–Dy(1)–O(4)	71.26(14)
O(3)–Dy(1)–O(5)	145.78(16)	O(4)–Dy(1)–O(5)	74.54(15)
O(1)–Dy(1)–N(1)	94.90(18)	O(1)–Dy(1)–N(4)	85.94(18)
O(2)–Dy(1)–N(1)	84.38(16)	O(2)–Dy(1)–N(4)	100.91(17)
O(3)–Dy(1)–N(1)	95.46(17)	O(3)–Dy(1)–N(4)	87.28(18)
O(4)–Dy(1)–N(1)	88.74(17)	O(4)–Dy(1)–N(4)	87.77(18)
O(5)–Dy(1)–N(1)	84.58(16)	O(5)–Dy(1)–N(4)	90.56(17)
N(1)–Dy(1)–N(4)	174.63(18)		
C(1)–Fe(1)–C(2)	90.6(2)	C(1)–Fe(1)–C(3)	89.1(3)
C(1)–Fe(1)–C(1)#1	180.0	C(1)–Fe(1)–C(2)#1	89.4(2)
C(1)–Fe(1)–C(3)#1	90.9(3)	C(2)–Fe(1)–C(3)	91.7(3)
C(2)–Fe(1)–C(2)#1	180.0	C(2)–Fe(1)–C(3)#1	88.3(3)
C(3)–Fe(1)–C(3)#1	180.0(3)	C(4)–Fe(2)–C(5)	88.6(3)
C(4)–Fe(2)–C(6)	89.6(3)	C(4)–Fe(2)–C(4)#2	180.0(2)
C(4)–Fe(2)–C(5)#2	91.4(3)	C(4)–Fe(2)–C(6)#2	90.4(3)
C(5)–Fe(2)–C(6)	90.0(3)	C(5)–Fe(2)–C(5)#2	180.0
C(5)–Fe(2)–C(6)#2	90.0(3)	C(6)–Fe(2)–C(6)#2	180.0
N(1)–C(1)–Fe(1)	179.3(6)	N(4)–C(4)–Fe(2)	177.1(6)
C(1)–N(1)–Dy(1)	177.6(6)	C(4)–N(4)–Dy(1)	167.3(5)

Symmetry codes： #1 –x+2,–y+2,–z+1, #2 –x+1,–y+1,–z.

Table S4 Selected bond lengths (Å) and angles (°) for **3**

Dy(1)–O(1)	2.302(5)	Dy(1)–O(2)	2.311(6)
Dy(1)–O(3)	2.328(7)	Dy(1)–O(4)	2.283(6)
Dy(1)–O(5)	2.276(6)	Dy(1)–N(1)	2.393(7)
Dy(1)–N(2)#1	2.378(8)		
Co(1)–C(1)	1.857(9)	Co(1)–C(2)	1.882(8)
Co(1)–C(3)	1.903(10)	Co(1)–C(4)	1.923(10)
Co(1)–C(5)	1.922(10)	Co(1)–C(6)	1.894(10)
O(1)–Dy(1)–O(2)	71.9(2)	O(1)–Dy(1)–O(3)	137.3(2)
O(1)–Dy(1)–O(4)	143.4(2)	O(1)–Dy(1)–O(5)	72.2(2)
O(2)–Dy(1)–O(3)	71.4(2)	O(2)–Dy(1)–O(4)	144.7(2)
O(2)–Dy(1)–O(5)	138.6(2)	O(3)–Dy(1)–O(4)	75.4(2)
O(3)–Dy(1)–O(5)	149.2(2)	O(4)–Dy(1)–O(5)	73.8(2)
O(1)–Dy(1)–N(1)	83.7(2)	O(1)–Dy(1)–N(2)#1	103.6(3)
O(2)–Dy(1)–N(1)	101.5(3)	O(2)–Dy(1)–N(2)#1	84.1(3)
O(3)–Dy(1)–N(1)	83.0(2)	O(3)–Dy(1)–N(2)#1	93.4(2)
O(4)–Dy(1)–N(1)	85.5(3)	O(4)–Dy(1)–N(2)#1	86.6(3)
O(5)–Dy(1)–N(1)	94.4(2)	O(5)–Dy(1)–N(2)#1	85.0(3)
N(1)–Dy(1)–N(2)#1	171.9(3)		
C(1)–Co(1)–C(2)	179.4(4)	C(1)–Co(1)–C(3)	89.7(3)
C(1)–Co(1)–C(4)	88.8(4)	C(1)–Co(1)–C(5)	89.2(3)
C(1)–Co(1)–C(6)	90.2(4)	C(2)–Co(1)–C(3)	89.7(3)
C(2)–Co(1)–C(4)	90.9(3)	C(2)–Co(1)–C(5)	91.3(3)
C(2)–Co(1)–C(6)	90.1(3)	C(3)–Co(1)–C(4)	89.5(4)
C(3)–Co(1)–C(5)	178.6(4)	C(3)–Co(1)–C(6)	88.3(4)
C(4)–Co(1)–C(5)	91.3(4)	C(4)–Co(1)–C(6)	177.6(4)
C(5)–Co(1)–C(6)	90.8(4)		
N(1)–C(1)–Co(1)	179.3(8)	N(2)–C(2)–Co(1)	179.3(8)
C(1)–N(1)–Dy(1)	174.6(7)	C(2)–N(2)–Dy(1)#2	179.2(8)

Symmetry codes： #1 x+1/2,y+1/2,z, #2 x–1/2,y–1/2,z.

Table S5 Hydrogen bonding geometry for **3**: lengths (Å) and angles (°)

D–H···A	d(D–H)	d(H···A)	d(D···A)	<(DHA)
O(6)–H(6A)···N(3)	0.98(3)	1.96(5)	2.886(13)	157(8)
O(6)–H(6B)···O(8)#5	0.97(3)	2.15(7)	2.793(14)	122(7)
O(7)–H(7A)···N(4)	0.96(3)	1.98(4)	2.916(12)	163(11)
O(7)–H(7B)···O(6)#3	0.96(3)	1.88(3)	2.836(15)	172(9)
O(8)–H(8A)···O(6)#4	0.97(3)	2.40(8)	2.793(14)	103(5)
O(8)–H(8B)···N(6)	0.97(3)	1.85(4)	2.806(12)	166(12)
O(9)–H(9A)···O(8)#3	0.94(3)	2.44(11)	2.851(13)	106(8)
O(9)–H(9B)···N(5)	0.95(3)	2.13(7)	3.004(13)	152(11)

Symmetry codes： #1 x+1/2,y+1/2,z, #2 x–1/2,y–1/2,z, #3 x–1/2,y+1/2,z, #4 x,–y–2,z+1/2, #5 x,–y–2,z–1/2.

Table S6 Selected bond lengths (Å) and angles (°) for **4**

Er(1)–O(1)	2.269(8)	Er(1)–O(2)	2.276(11)
Er(1)–O(3)	2.298(11)	Er(1)–O(4)	2.284(10)
Er(1)–O(5)	2.263(9)	Er(1)–N(1)	2.347(11)
Er(1)–N(2)#1	2.339(12)		
Fe(1)–C(1)	1.899(14)	Fe(1)–C(2)	1.926(12)
Fe(1)–C(3)	1.933(16)	Fe(1)–C(4)	1.970(16)
Fe(1)–C(5)	1.958(14)	Fe(1)–C(6)	1.921(16)
O(1)–Er(1)–O(2)	71.9(3)	O(1)–Er(1)–O(3)	138.2(4)
O(1)–Er(1)–O(4)	143.5(3)	O(1)–Er(1)–O(5)	71.8(3)
O(2)–Er(1)–O(3)	71.4(4)	O(2)–Er(1)–O(4)	144.6(3)
O(2)–Er(1)–O(5)	138.8(3)	O(3)–Er(1)–O(4)	75.1(4)
O(3)–Er(1)–O(5)	149.0(3)	O(4)–Er(1)–O(5)	73.9(3)
O(1)–Er(1)–N(1)	83.8(3)	O(1)–Er(1)–N(2)#1	102.2(4)
O(2)–Er(1)–N(1)	100.7(4)	O(2)–Er(1)–N(2)#1	83.9(4)
O(3)–Er(1)–N(1)	83.9(4)	O(3)–Er(1)–N(2)#1	93.2(4)
O(4)–Er(1)–N(1)	86.4(4)	O(4)–Er(1)–N(2)#1	87.1(4)
O(5)–Er(1)–N(1)	94.1(4)	O(5)–Er(1)–N(2)#1	85.3(4)
N(1)–Er(1)–N(2)#1	173.4(5)		
C(1)–Fe(1)–C(2)	180.0(8)	C(1)–Fe(1)–C(3)	90.6(5)
C(1)–Fe(1)–C(4)	89.3(5)	C(1)–Fe(1)–C(5)	89.1(5)
C(1)–Fe(1)–C(6)	90.4(6)	C(2)–Fe(1)–C(3)	89.4(5)
C(2)–Fe(1)–C(4)	90.6(5)	C(2)–Fe(1)–C(5)	90.9(5)
C(2)–Fe(1)–C(6)	89.7(6)	C(3)–Fe(1)–C(4)	88.0(6)
C(3)–Fe(1)–C(5)	179.5(6)	C(3)–Fe(1)–C(6)	88.1(7)
C(4)–Fe(1)–C(5)	92.4(6)	C(4)–Fe(1)–C(6)	176.0(7)
C(5)–Fe(1)–C(6)	91.5(6)		
N(1)–C(1)–Fe(1)	177.6(12)	N(2)–C(2)–Fe(1)	178.8(12)
C(1)–N(1)–Er(1)	176.6(10)	C(2)–N(2)–Er(1)#2	179.4(14)

Symmetry codes： #1 x–1/2,y–1/2,z, #2 x+1/2,y+1/2,z.

Table S7 Hydrogen bonding geometry for **4**: lengths (Å) and angles (°)

D–H···A	d(D–H)	d(H···A)	d(D···A)	<(DHA)
O(6)–H(6A)···N(3)	0.96(3)	2.00(10)	2.886(19)	152(18)
O(7)–H(7A)···N(4)	0.96(3)	2.10(13)	2.90(2)	139(16)
O(8)–H(8B)···N(6)	0.96(3)	2.04(17)	2.83(2)	138(20)
O(9)–H(9B)···N(5)	0.96(3)	2.21(10)	3.00(2)	139(13)

Symmetry codes： #1 x–1/2,y–1/2,z, #2 x+1/2,y+1/2,z.

Table S8 Selected bond lengths (Å) and angles (°) for **5**

Er(1)–O(1)	2.280(13)	Er(1)–O(2)	2.279(13)
Er(1)–O(3)	2.325(14)	Er(1)–O(4)	2.269(12)
Er(1)–O(5)	2.276(12)	Er(1)–N(1)	2.360(12)
Er(1)–N(2)#1	2.353(12)		
Co(1)–C(1)	1.872(15)	Co(1)–C(2)	1.862(14)
Co(1)–C(3)	1.91(2)	Co(1)–C(4)	1.932(17)
Co(1)–C(5)	1.897(18)	Co(1)–C(6)	1.90(2)
O(1)–Er(1)–O(2)	72.1(5)	O(1)–Er(1)–O(3)	137.2(5)
O(1)–Er(1)–O(4)	143.7(5)	O(1)–Er(1)–O(5)	71.8(4)
O(2)–Er(1)–O(3)	70.9(5)	O(2)–Er(1)–O(4)	144.2(5)
O(2)–Er(1)–O(5)	138.1(5)	O(3)–Er(1)–O(4)	75.6(5)
O(3)–Er(1)–O(5)	149.9(5)	O(4)–Er(1)–O(5)	74.3(5)
O(1)–Er(1)–N(1)	84.7(5)	O(1)–Er(1)–N(2)#1	103.8(5)
O(2)–Er(1)–N(1)	102.3(5)	O(2)–Er(1)–N(2)#1	83.7(5)
O(3)–Er(1)–N(1)	82.8(5)	O(3)–Er(1)–N(2)#1	92.9(5)
O(4)–Er(1)–N(1)	85.5(5)	O(4)–Er(1)–N(2)#1	85.7(5)
O(5)–Er(1)–N(1)	94.9(5)	O(5)–Er(1)–N(2)#1	84.8(5)
N(1)–Er(1)–N(2)#1	170.9(5)		
C(1)–Co(1)–C(2)	178.6(8)	C(1)–Co(1)–C(3)	90.7(7)
C(1)–Co(1)–C(4)	88.9(6)	C(1)–Co(1)–C(5)	88.7(7)
C(1)–Co(1)–C(6)	91.8(8)	C(2)–Co(1)–C(3)	90.0(7)
C(2)–Co(1)–C(4)	90.0(6)	C(2)–Co(1)–C(5)	90.6(6)
C(2)–Co(1)–C(6)	89.4(8)	C(3)–Co(1)–C(4)	87.9(7)
C(3)–Co(1)–C(5)	179.3(8)	C(3)–Co(1)–C(6)	89.8(10)
C(4)–Co(1)–C(5)	91.9(6)	C(4)–Co(1)–C(6)	177.6(10)
C(5)–Co(1)–C(6)	90.5(9)		
N(1)–C(1)–Co(1)	179.0(16)	N(2)–C(2)–Co(1)	178.5(15)
C(1)–N(1)–Er(1)	173.5(13)	C(2)–N(2)–Er(1)#2	177.5(12)

Symmetry codes： #1 x–1/2,y–1/2,z, #2 x+1/2,y+1/2,z.

Table S9 Hydrogen bonding geometry for **5**: lengths (Å) and angles (°)

D–H···A	d(D–H)	d(H···A)	d(D···A)	<(DHA)
O(6)–H(6B)···N(3)	0.96(3)	2.2(2)	2.88(3)	123(20)
O(7)–H(7A)···N(4)	0.97(3)	2.21(9)	2.86(2)	123(7)
O(8)–H(8A)···N(6)	0.97(3)	2.22(16)	2.80(2)	118(13)

Symmetry codes： #1 x–1/2,y–1/2,z, #2 x+1/2,y+1/2,z.

Table S10 Continuous shape measures (CShM) for **1**–**5** using SHAPE 2.1

	1	**2**	**3**	**4**	**5**
HP-7	34.916	34.187	34.847	34.851	34.901
HPY-7	23.293	24.851	23.002	23.449	22.951
PBPY-7	1.065	0.619	1.198	1.012	1.255
COC-7	4.348	5.015	4.086	4.366	3.970
CTPR-7	2.891	3.949	2.679	2.916	2.582
JPBPY-7	5.222	4.792	5.466	5.143	5.407
JETPY-7	22.794	22.165	22.814	22.851	22.758

HP-7 = (D_{7h}) Heptagon
HPY-7 = (C_{6v}) Hexagonal pyramid
PBPY-7 = (D_{5h}) Pentagonal bipyramid
COC-7 = (C_{3v}) Capped octahedron
CTPR-7 = (C_{2v}) Capped trigonal prism
JPBPY-7 = (D_{5h}) Johnson pentagonal bipyramid J13
JETPY-7 = (C_{3v}) Johnson elongated triangular pyramid J7

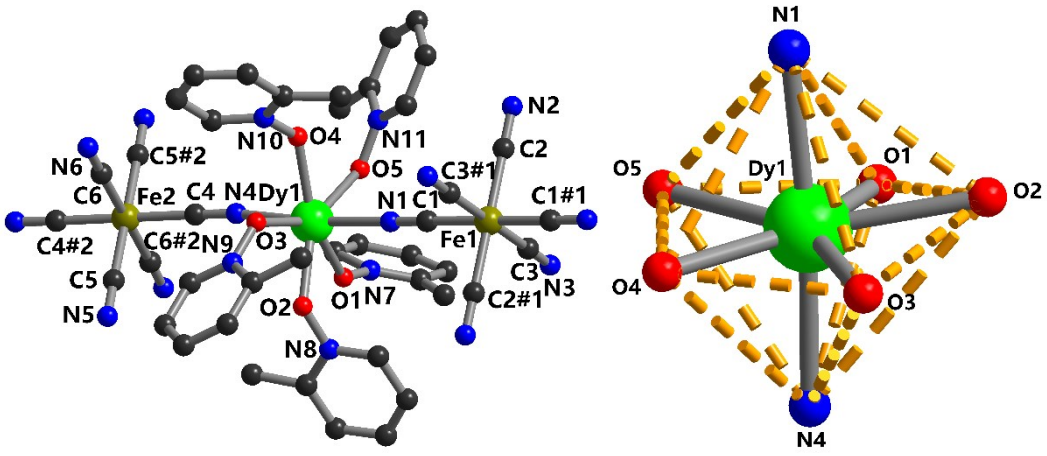

(a) (b)

Fig. S1. (a) View of the local molecular structure of compound **2**. (b) The pentagonal-bipyramidal (D_{5h}) coordination geometry around the Dy^{III} ion in compound **2**. Color code: Dy, green; Fe, dark yellow; C, black; N, blue; O, red. Hydrogen atoms are omitted for clarity.

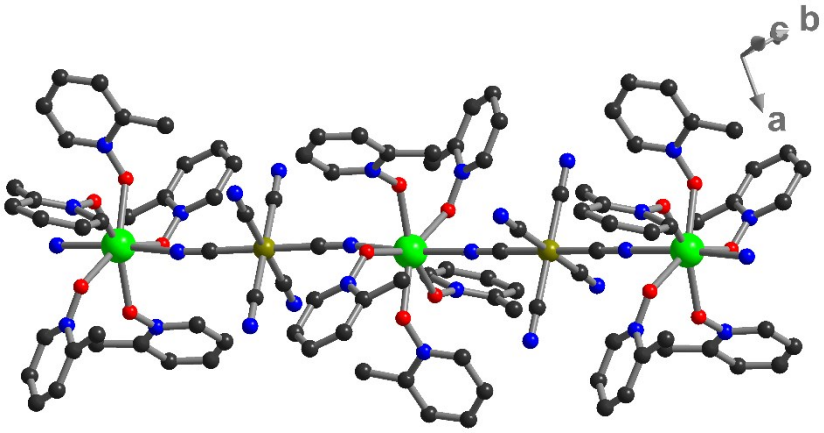

Fig. S2. View of the linear chain structure of compound **2**.

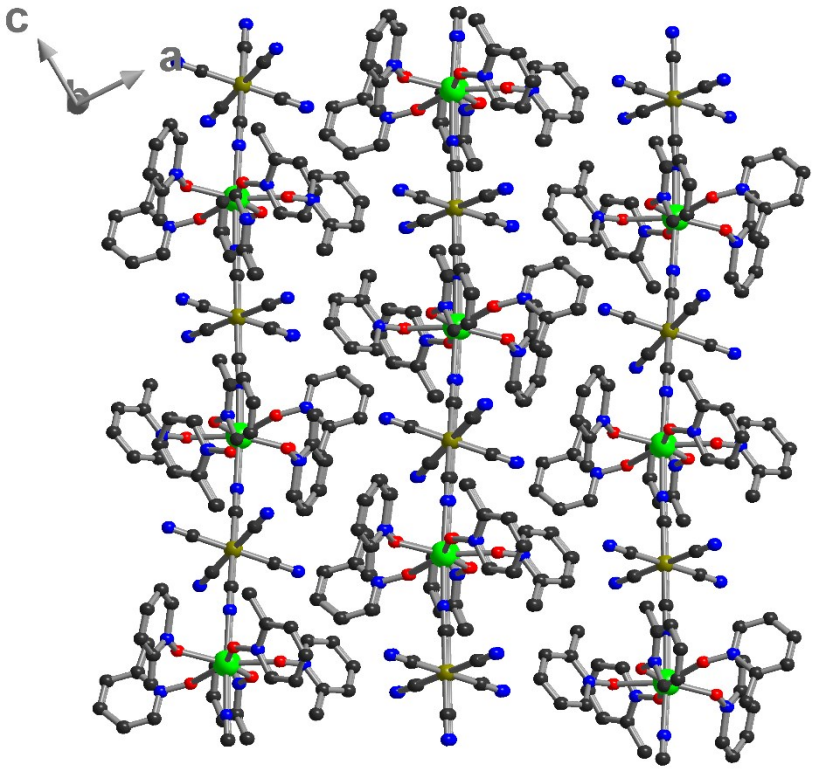

Fig. S3. View of the packing pattern of compound **2** along the *b* direction.

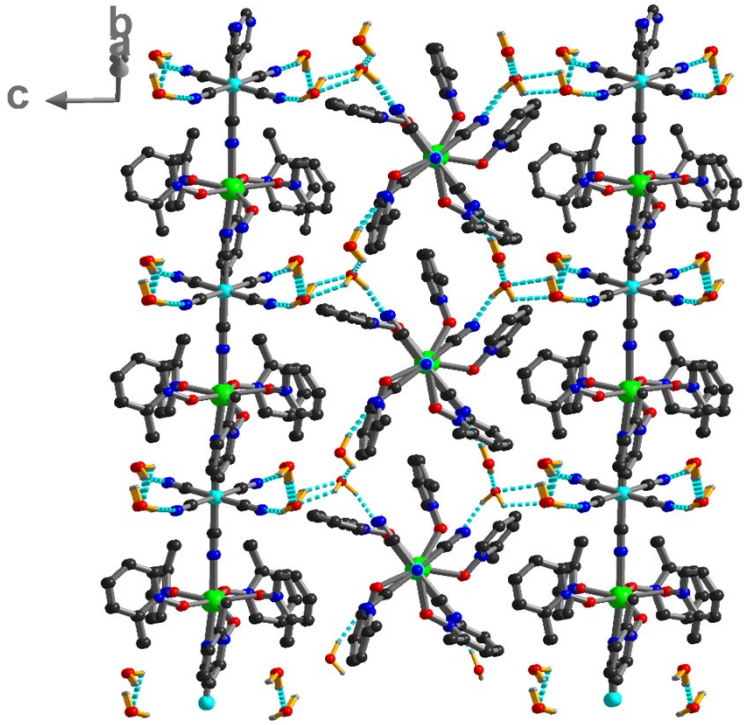

Fig. S4. View of the packing pattern of compound **3** along the *a*–*b* direction.

3. Powder XRD Analyses

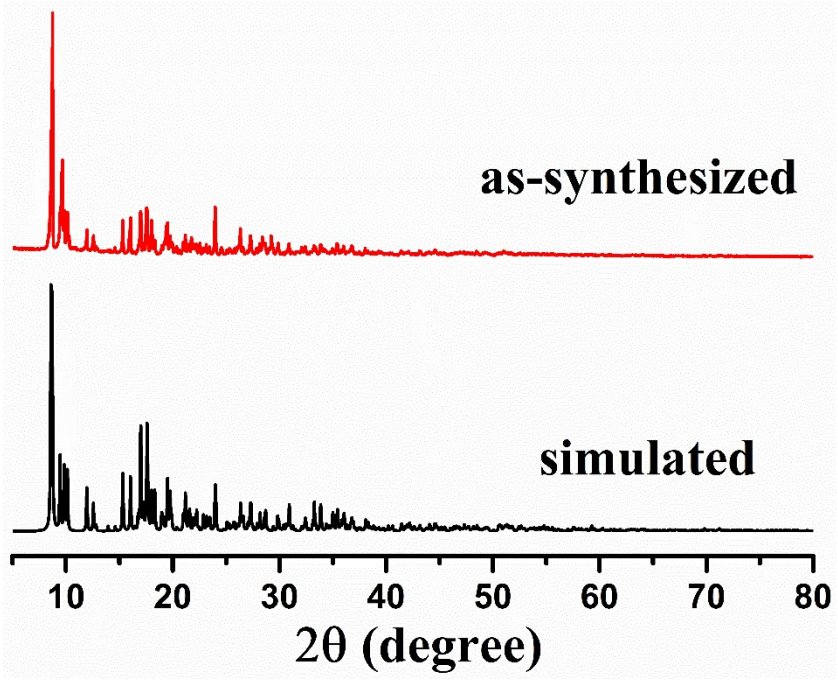

Fig. S5. Powder X-ray diffraction pattern of compound **1** for the as-synthesized sample and the simulated one.

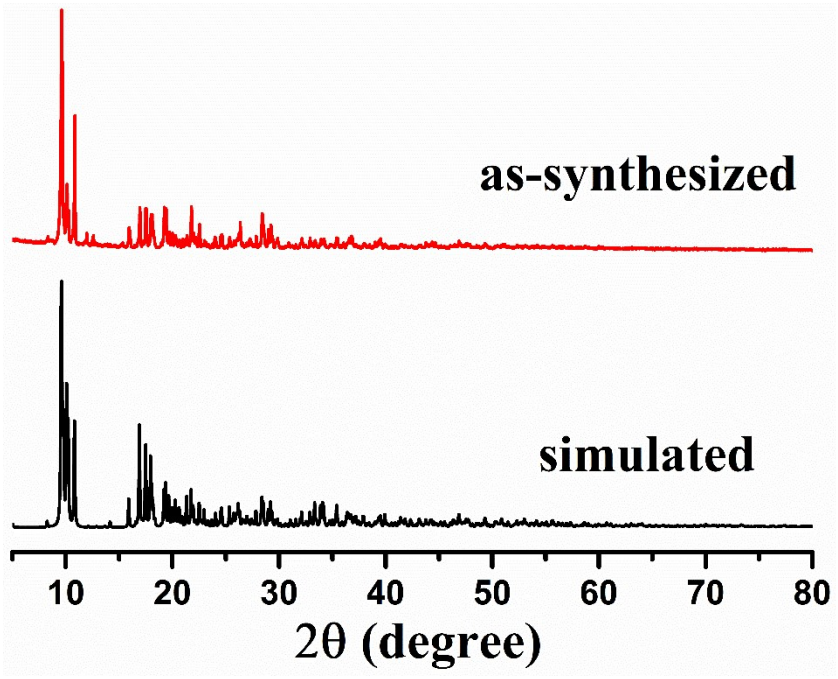

Fig. S6. Powder X-ray diffraction pattern of compound **2** for the as-synthesized sample and the simulated one.

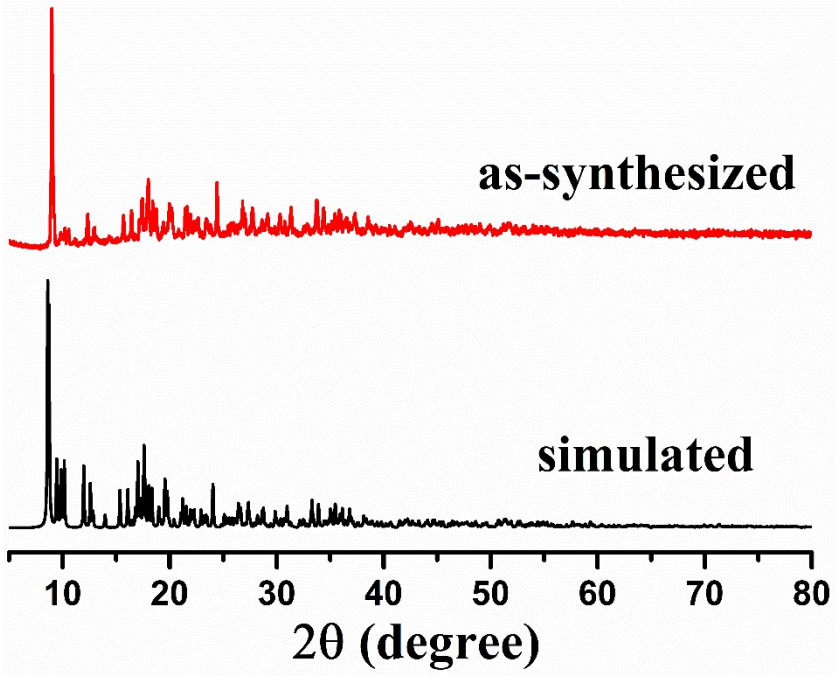

Fig. S7. Powder X-ray diffraction pattern of compound **3** for the as-synthesized sample and the simulated one.

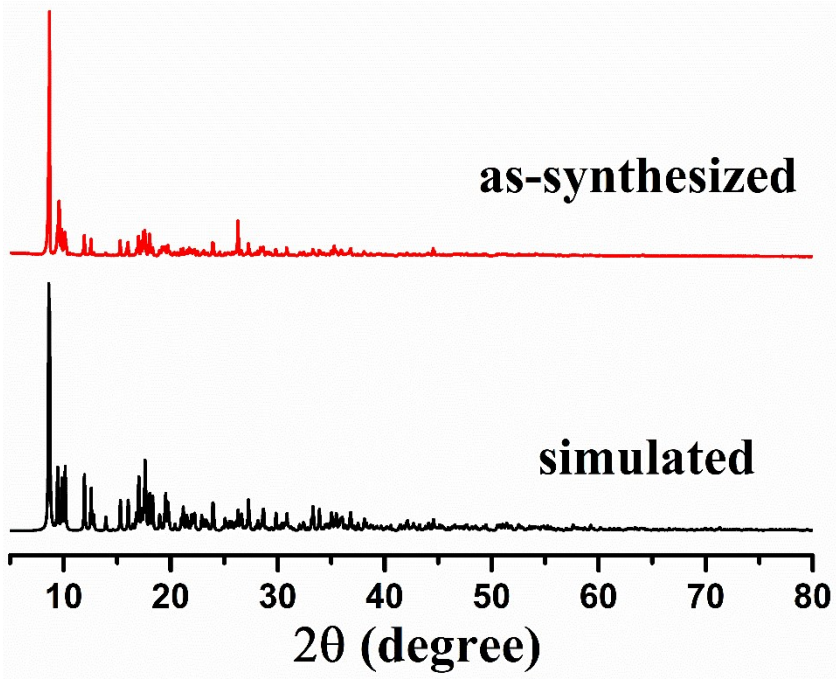

Fig. S8. Powder X-ray diffraction pattern of compound **4** for the as-synthesized sample and the simulated one.

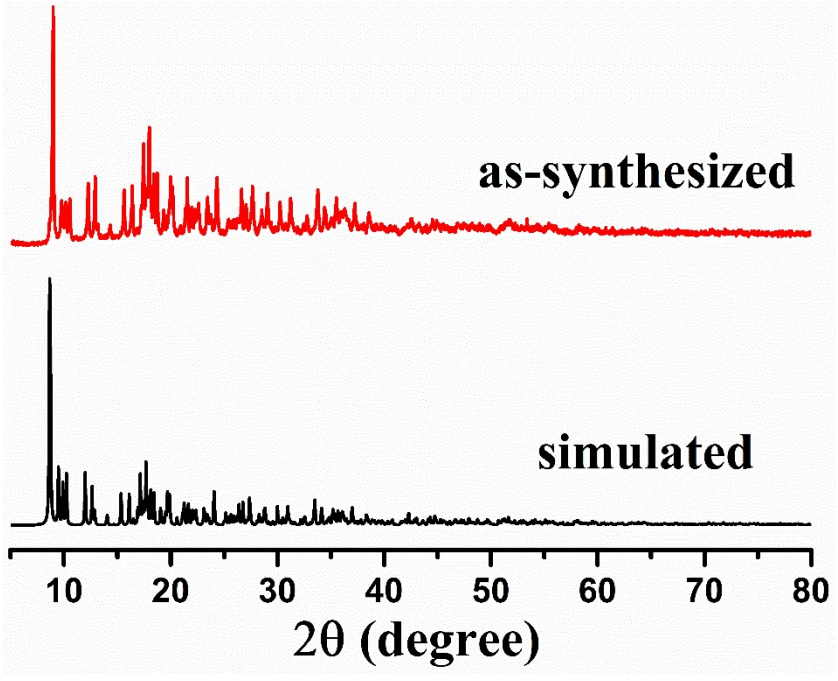

Fig. S9. Powder X-ray diffraction pattern of compound **5** for the as-synthesized sample and the simulated one.

4. Magnetic Properties

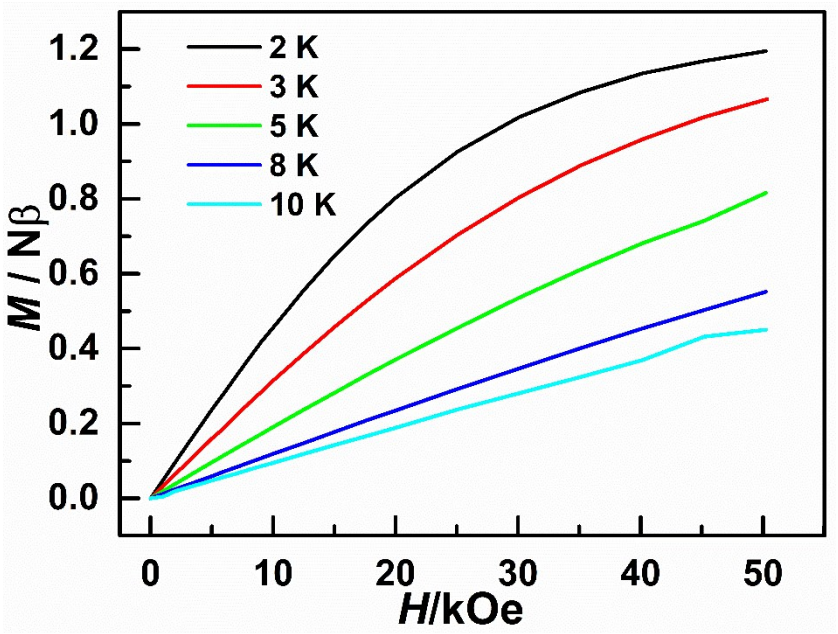

Fig. S10. Field dependence of the magnetization at the temperatures of 2, 3, 5, 8 and 10 K for a polycrystalline sample of **1**.

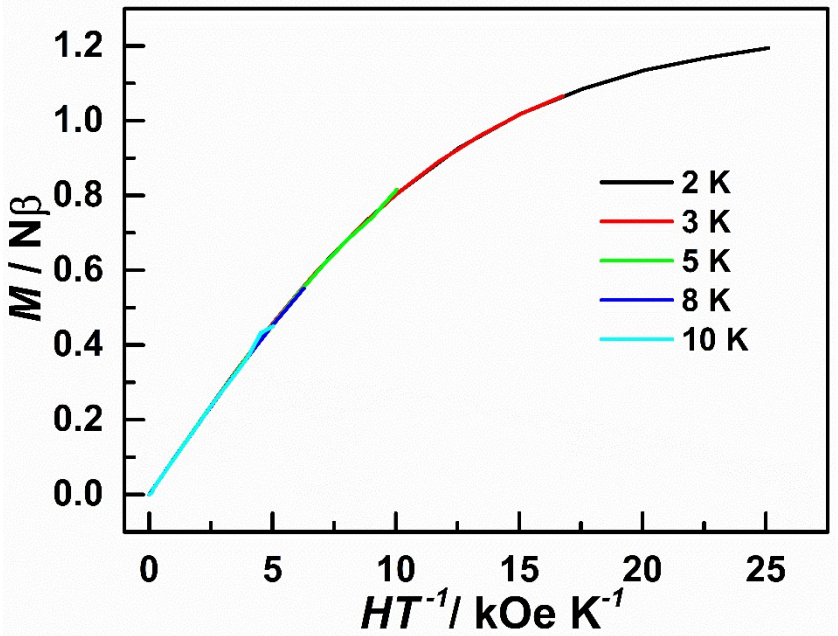

Fig. S11. Plots of the reduced magnetization *M* vs *H*/*T* at the temperatures of 2, 3, 5, 8 and 10 K for a polycrystalline sample of **1**.

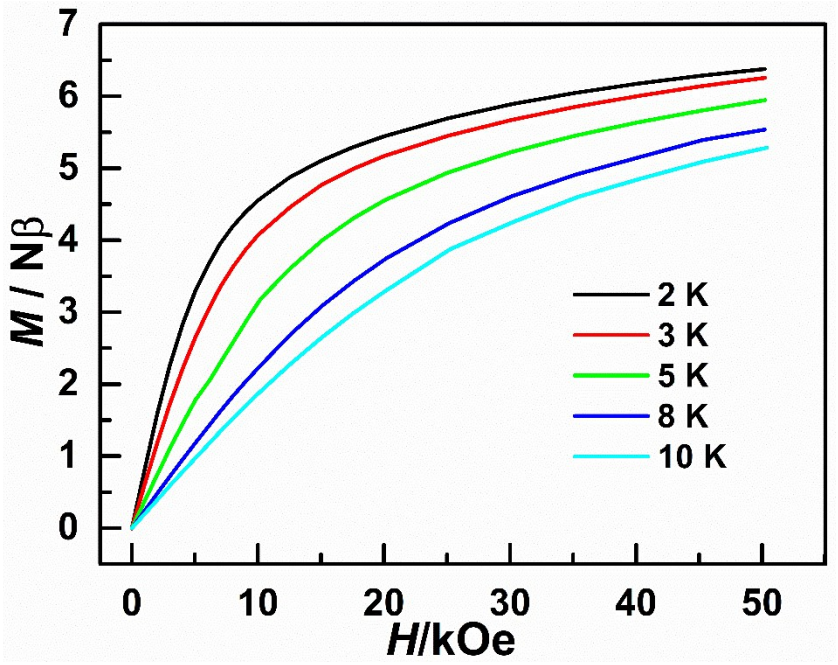

Fig. S12. Field dependence of the magnetization at the temperatures of 2, 3, 5, 8 and 10 K for a polycrystalline sample of **2**.

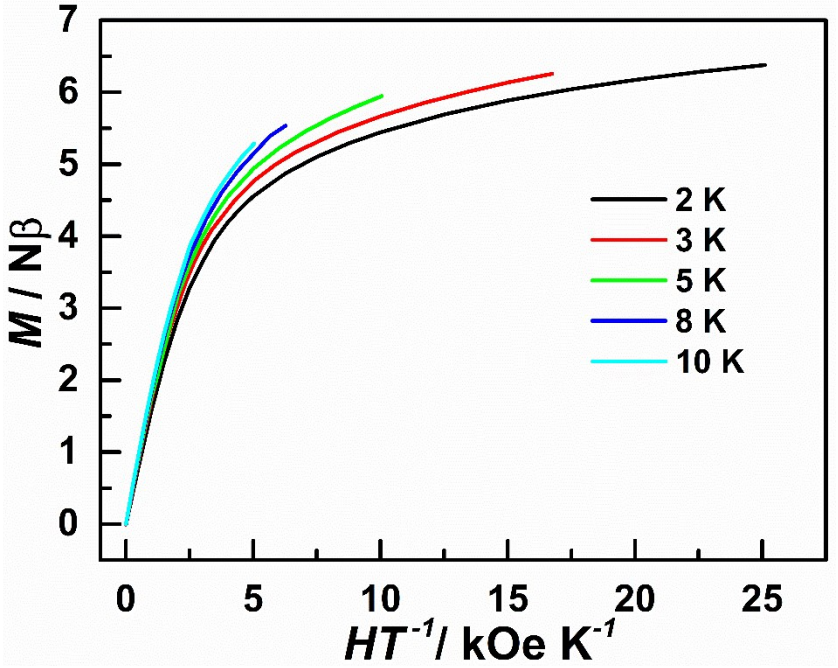

Fig. S13. Field dependence of the magnetization at the temperatures of 2, 3, 5, 8 and 10 K for a polycrystalline sample of **2**.

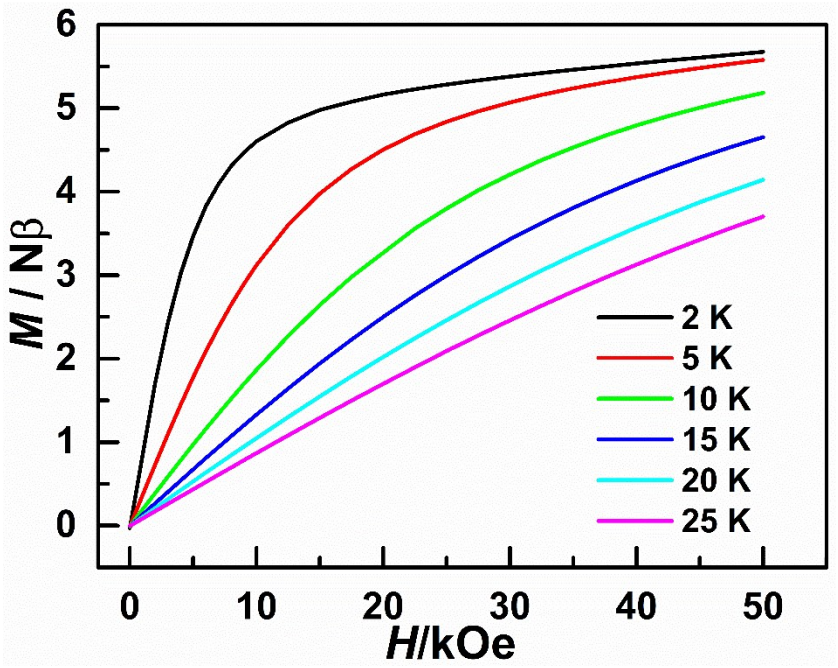

Fig. S14. Field dependence of the magnetization at the temperatures of 2, 5, 10, 15, 20 and 25 K for a polycrystalline sample of **3**.

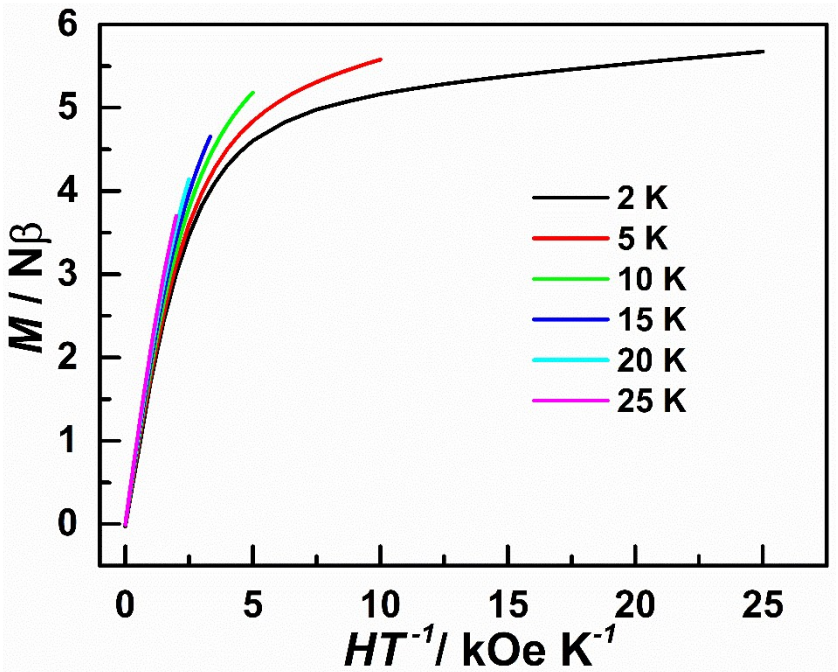

Fig. S15. Field dependence of the magnetization at the temperatures of 2, 5, 10, 15, 20 and 25 K for a polycrystalline sample of **3**.

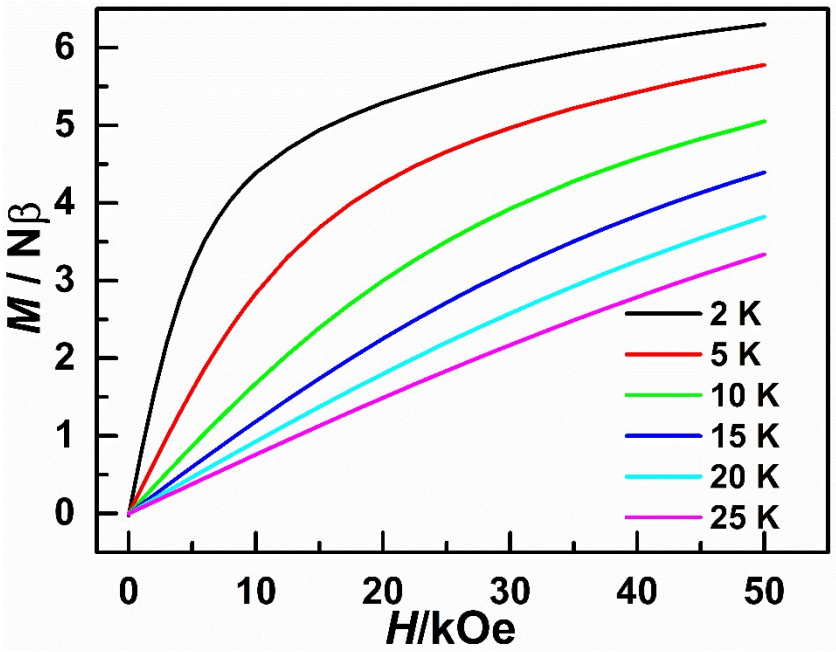

Fig. S16. Field dependence of the magnetization at the temperatures of 2, 5, 10, 15, 20 and 25 K for a polycrystalline sample of **4**.

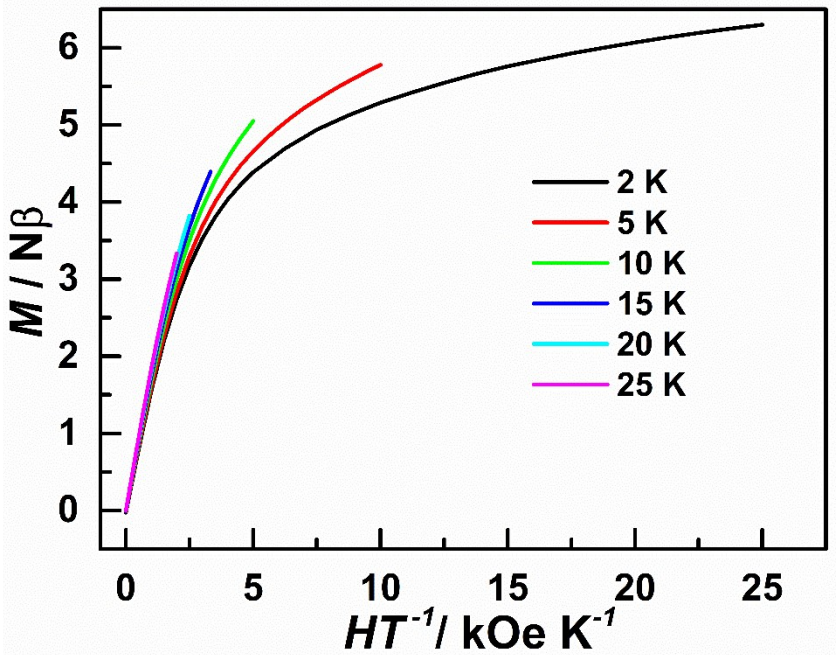

Fig. S17. Field dependence of the magnetization at the temperatures of 2, 5, 10, 15, 20 and 25 K for a polycrystalline sample of **4**.

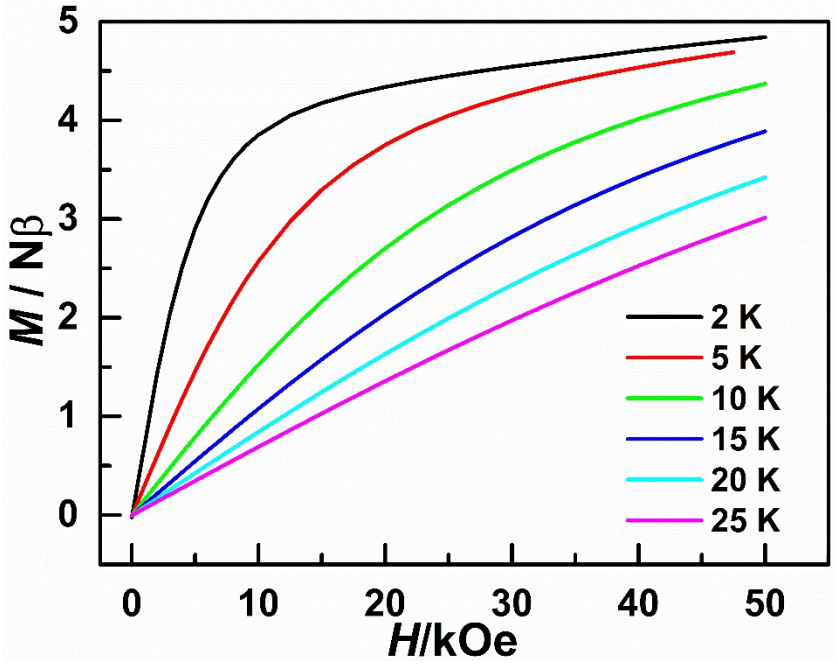

Fig. S18. Field dependence of the magnetization at the temperatures of 2, 5, 10, 15, 20 and 25 K for a polycrystalline sample of **5**.

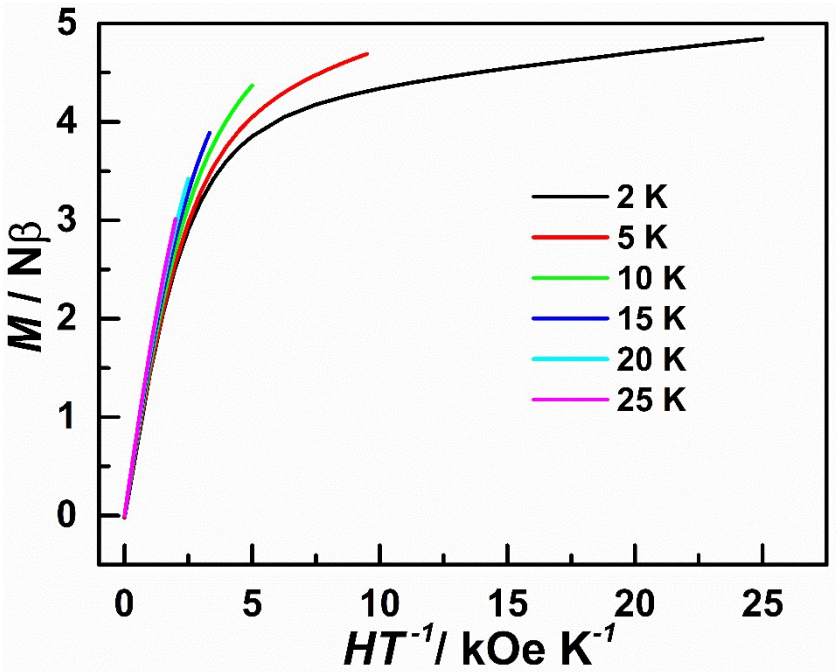

Fig. S19. Field dependence of the magnetization at the temperatures of 2, 5, 10, 15, 20 and 25 K for a polycrystalline sample of **5**.

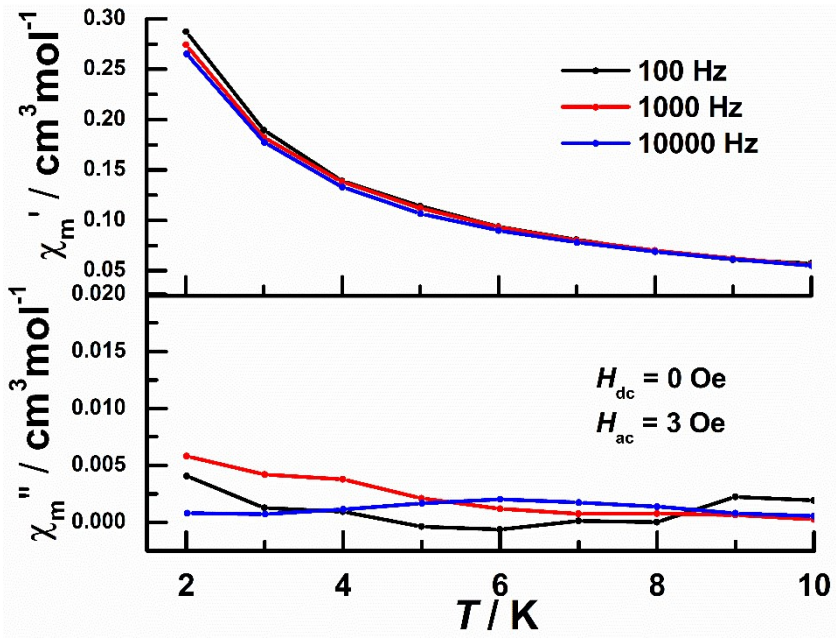

Fig. S20. Temperature dependence of the χ' and χ'' ac susceptibility components for compound **1** under zero dc field at indicated ac frequencies.

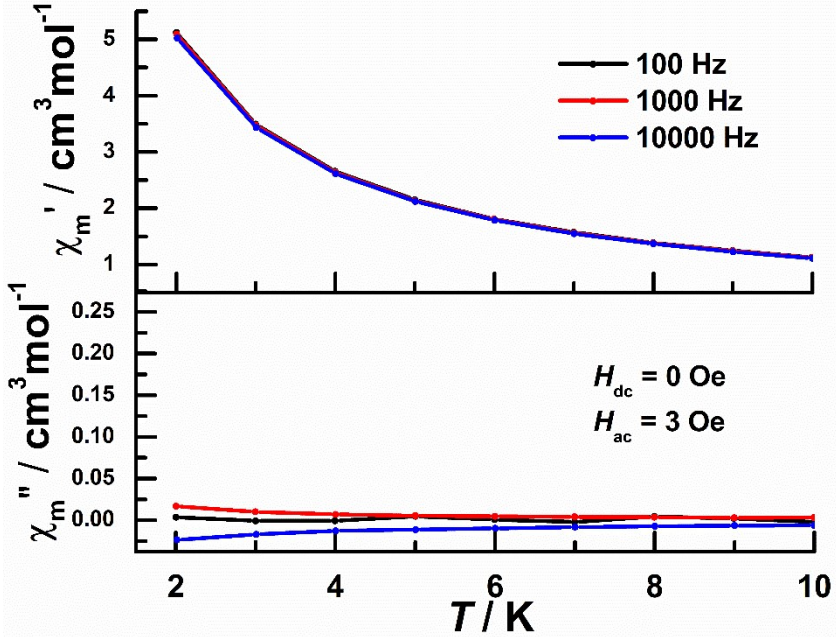

Fig. S21. Temperature dependence of the χ' and χ'' ac susceptibility components for compound **2** under zero dc field at indicated ac frequencies.

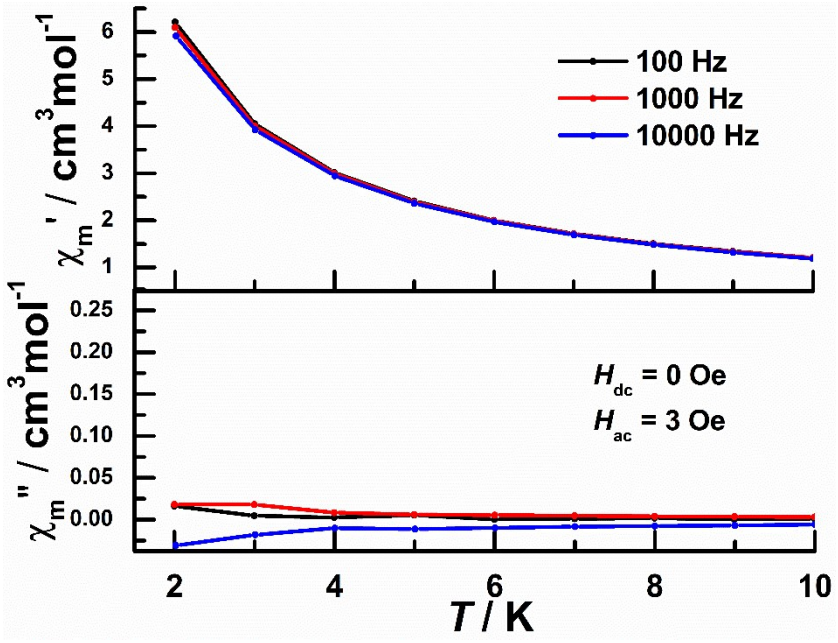

Fig. S22. Temperature dependence of the χ' and χ'' ac susceptibility components for compound **3** under zero dc field at indicated ac frequencies.

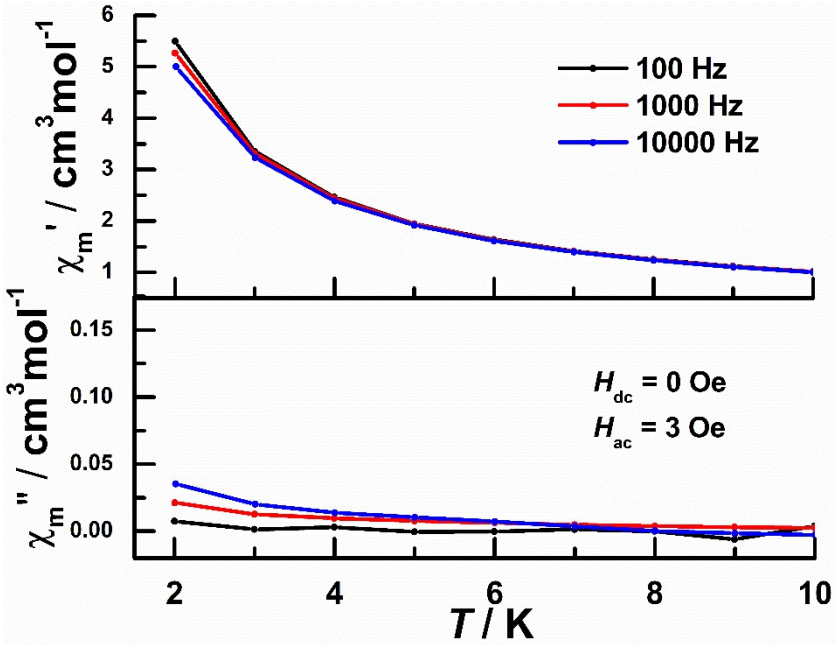

Fig. S23. Temperature dependence of the χ' and χ'' ac susceptibility components for compound **4** under zero dc field at indicated ac frequencies.

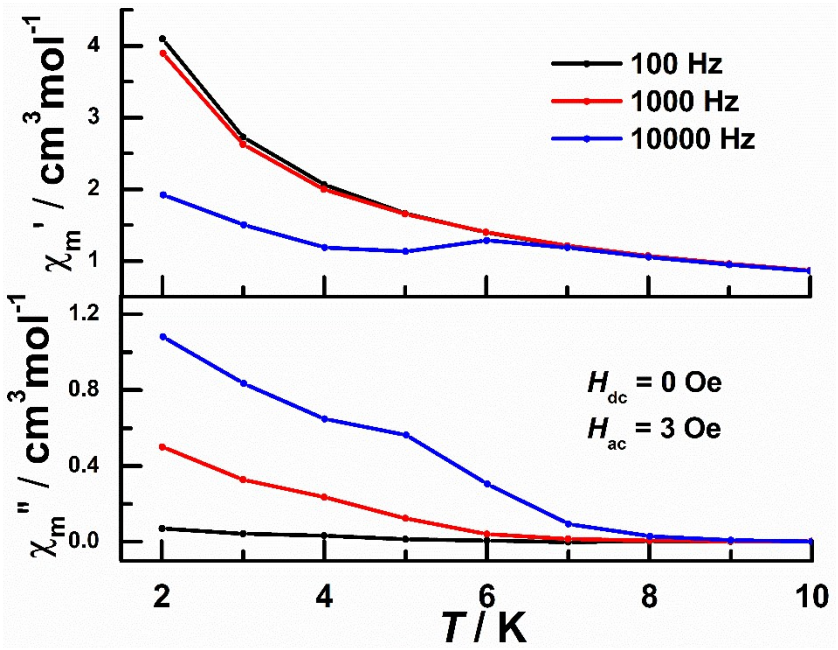

Fig. S24. Temperature dependence of the χ' and χ'' ac susceptibility components for compound **5** under zero dc field at indicated ac frequencies.

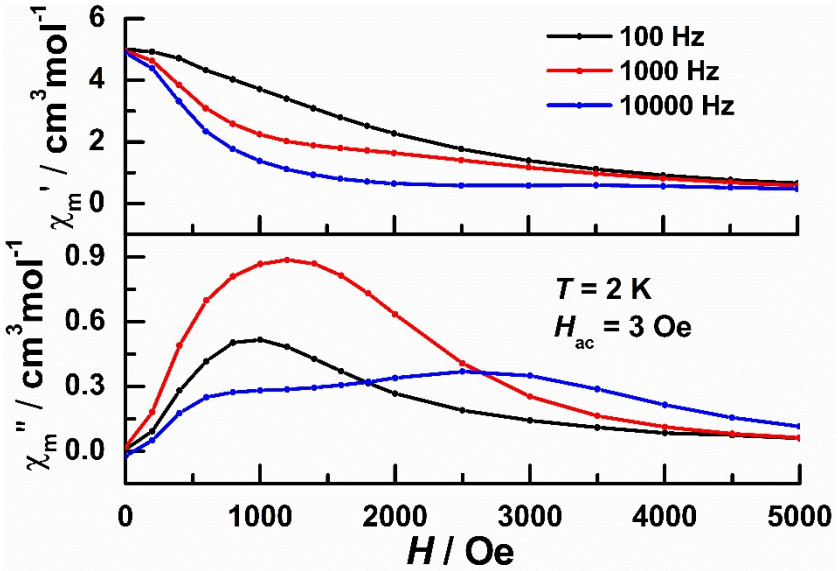

Fig. S25. Field dependence of the χ' and χ'' ac susceptibilities components for **2** with f = 100, 1000 and 10000 Hz.

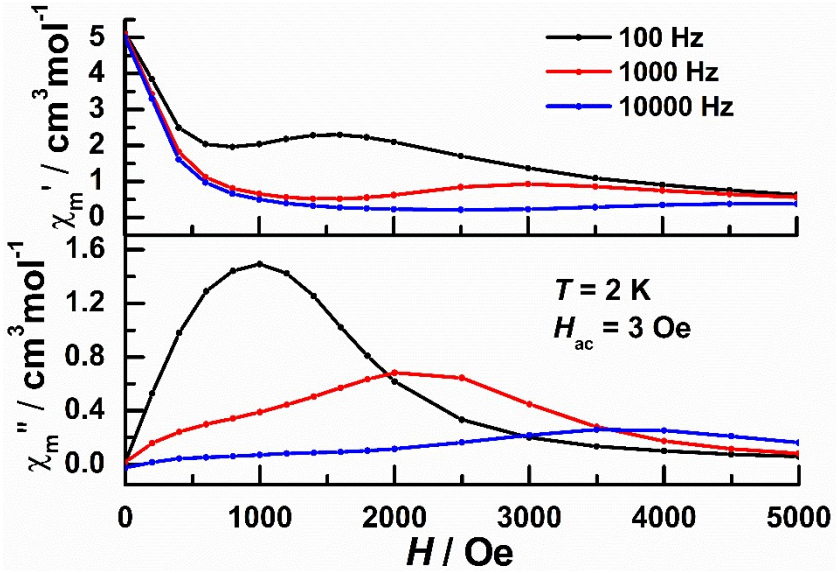

Fig. S26. Field dependence of the χ' and χ'' ac susceptibilities components for **3** with f = 100, 1000 and 10000 Hz.

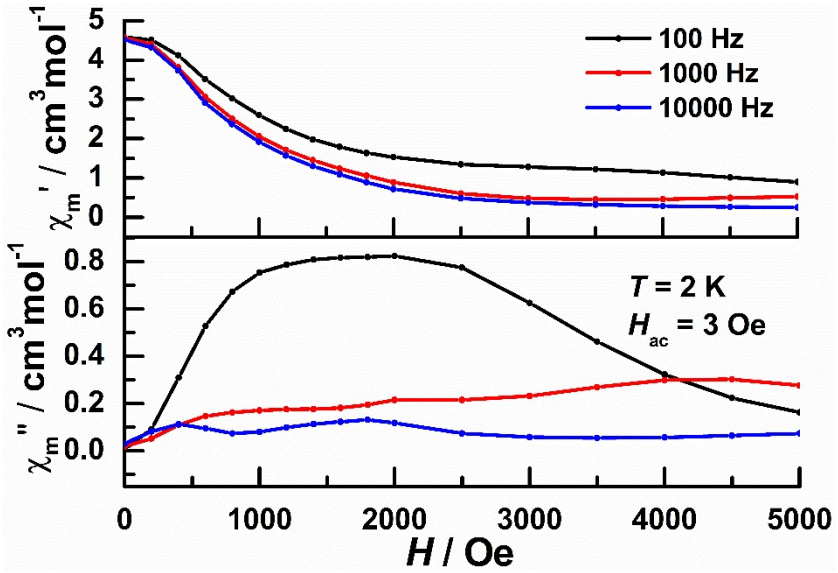

Fig. S27. Field dependence of the χ' and χ'' ac susceptibilities components for **4** with f = 100, 1000 and 10000 Hz.

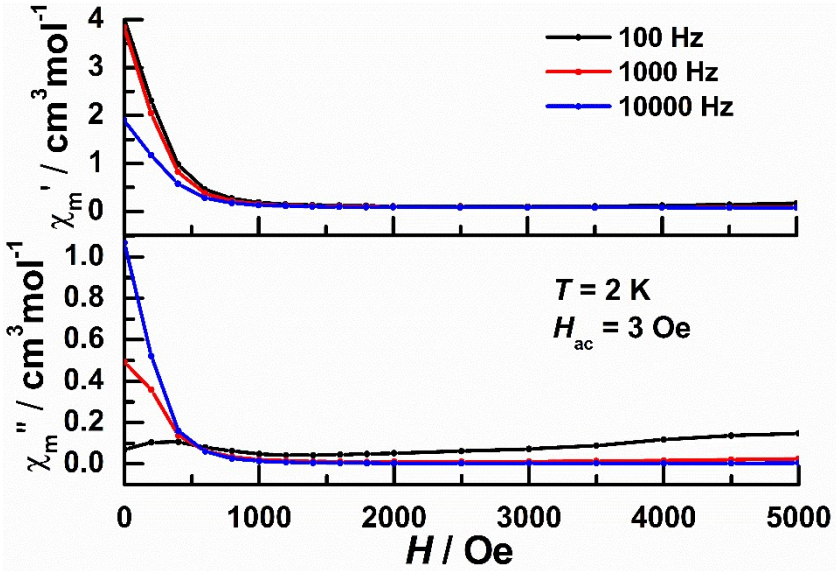

Fig. S28. Field dependence of the χ' and χ'' ac susceptibilities components for **5** with f = 100, 1000 and 10000 Hz.

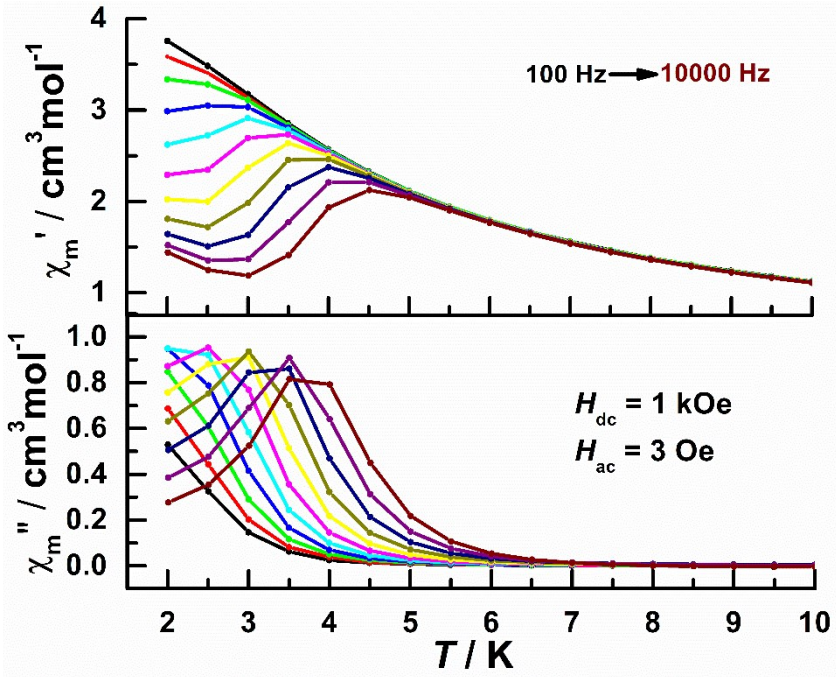

Fig. S29. Temperature dependence of the χ' and χ'' ac susceptibility components for **2** under a 1 kOe dc field at indicated ac frequencies.

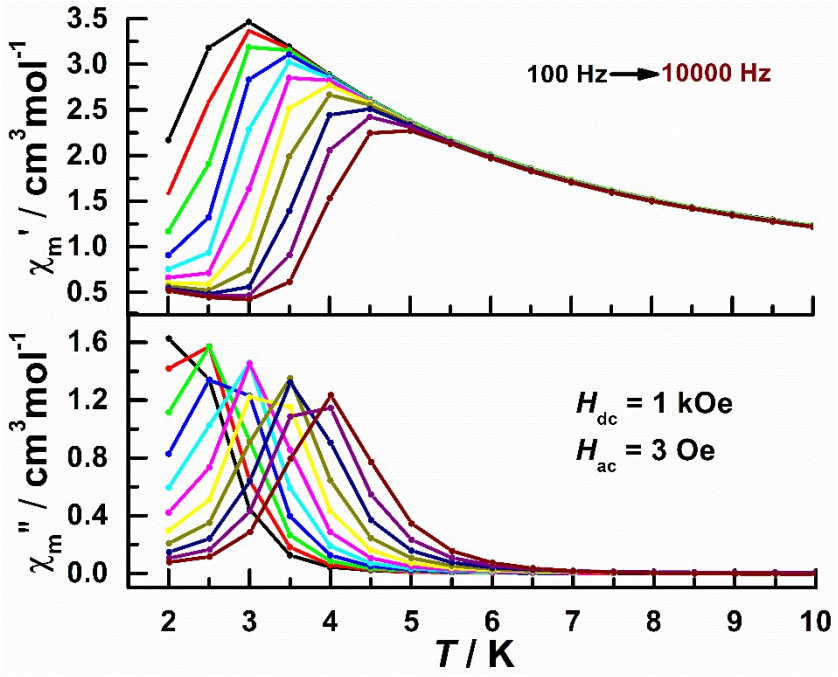

Fig. S30. Temperature dependence of the χ' and χ'' ac susceptibility components for **3** under a 1 kOe dc field at indicated ac frequencies.

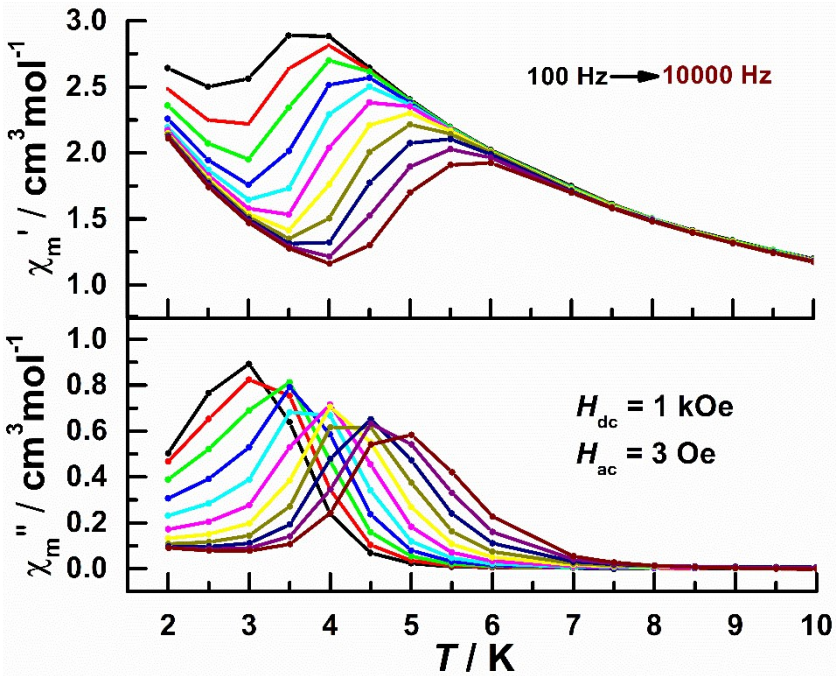

Fig. S31. Temperature dependence of the χ' and χ'' ac susceptibility components for **4** under a 1 kOe dc field at indicated ac frequencies.

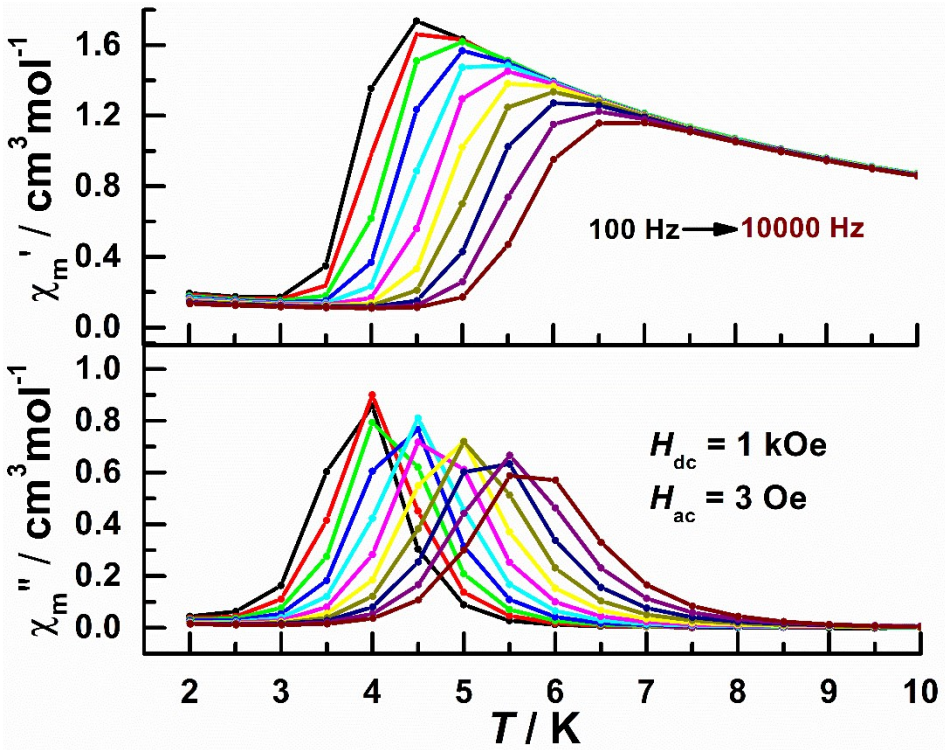

Fig. S32. Temperature dependence of the χ' and χ'' ac susceptibility components for **5** under a 1 kOe dc field at indicated ac frequencies.

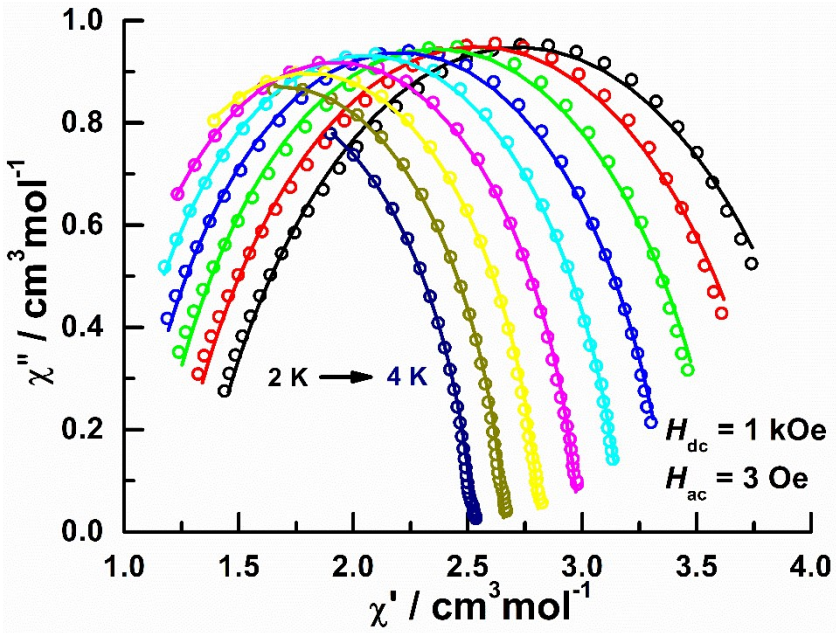

Fig. S33. The Cole−Cole plots in the range of 2−4 K (0.25 K as a step) for compound **2** under a 1 kOe dc field. The solid lines are the least-square fitting of the data to a distribution of single relaxation processes with the generalized Debye model.

Table S11 Relaxation parameters from the best fitting of the Cole−Cole diagrams in the range of 2−4 K by the generalized Debye model under a 1 kOe dc field for **2**.

T(K)	χ_S(cm^3 mol^{-1})	χ_T(cm^3 mol^{-1})	τ(s)	α
2.00	1.31	4.13	0.28E-3	0.247
2.25	1.20	3.88	0.22E-3	0.216
2.50	1.11	3.62	0.16E-3	0.180
2.75	1.02	3.38	0.11E-3	0.145
3.00	0.95	3.17	0.70E-4	0.112
3.25	0.87	2.99	0.43E-4	0.090
3.50	0.80	2.81	0.27E-4	0.074
3.75	0.71	2.66	0.16E-4	0.073
4.00	0.60	2.52	0.10E-4	0.084

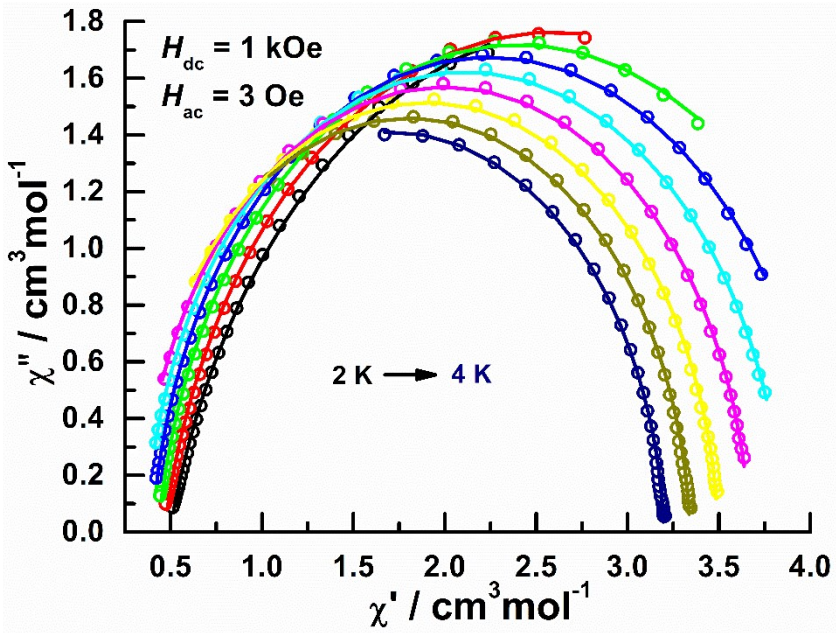

Fig. S34. The Cole−Cole plots in the range of 2−4 K (0.25 K as a step) for **3** under a 1 kOe dc field. The solid lines are the least-square fitting of the data to a distribution of single relaxation processes with the generalized Debye model.

Table S12 Relaxation parameters from the best fitting of the Cole−Cole diagrams in the range of 2−4 K by the generalized Debye model under a 1 kOe dc field for **3**.

T(K)	χ_S(cm^3 mol^{-1})	χ_T(cm^3 mol^{-1})	τ(s)	α
2.00	0.50	5.12	0.23E-2	0.162
2.25	0.47	4.72	0.14E-2	0.119
2.50	0.43	4.37	0.80E-3	0.086
2.75	0.40	4.09	0.41E-3	0.061
3.00	0.36	3.86	0.20E-3	0.047
3.25	0.33	3.67	0.10E-3	0.039
3.50	0.30	3.50	0.53E-4	0.034
3.75	0.27	3.34	0.29E-4	0.032
4.00	0.21	3.20	0.16E-4	0.036

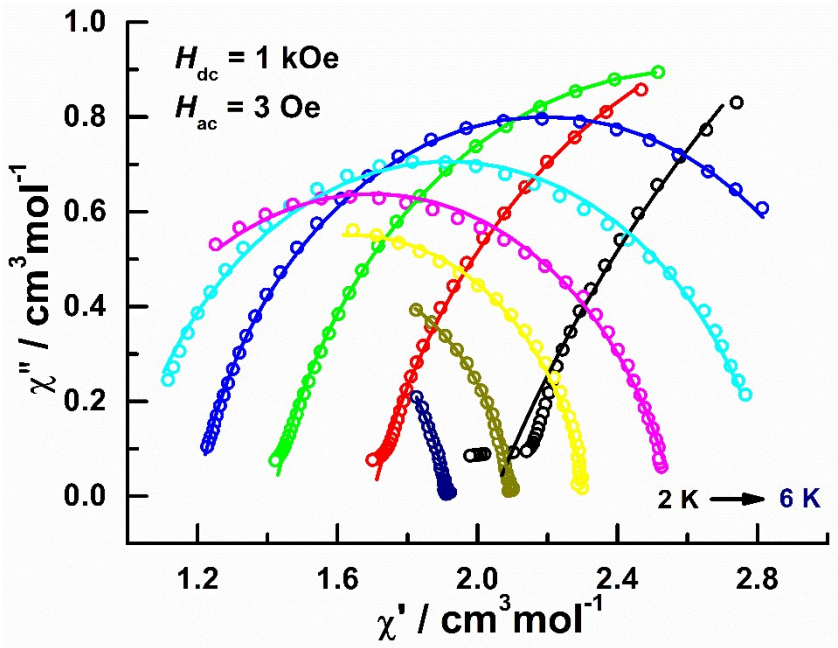

Fig. S35. The Cole−Cole plots in the range of 2−6 K (0.5 K as a step) for **4** under a 1 kOe dc field. The solid lines are the least-square fitting of the data to a distribution of single relaxation processes with the generalized Debye model.

Table S13 Relaxation parameters from the best fitting of the Cole−Cole diagrams in the range of 2−6 K by the generalized Debye model under a 1 kOe dc field for **4**.

T(K)	χ_S(cm^3 mol^{-1})	χ_T(cm^3 mol^{-1})	τ(s)	α
2.0	2.04	7.41	0.15E-1	0.317
2.5	1.70	4.53	0.37E-2	0.208
3.0	1.42	3.78	0.18E-2	0.173
3.5	1.20	3.19	0.56E-3	0.137
4.0	0.99	2.84	0.14E-3	0.172
4.5	0.84	2.56	0.39E-4	0.186
5.0	0.97	2.31	0.17E-4	0.122
5.5	1.03	2.09	0.82E-5	0.088
6.0	0.64	1.91	0.23E-5	0.144

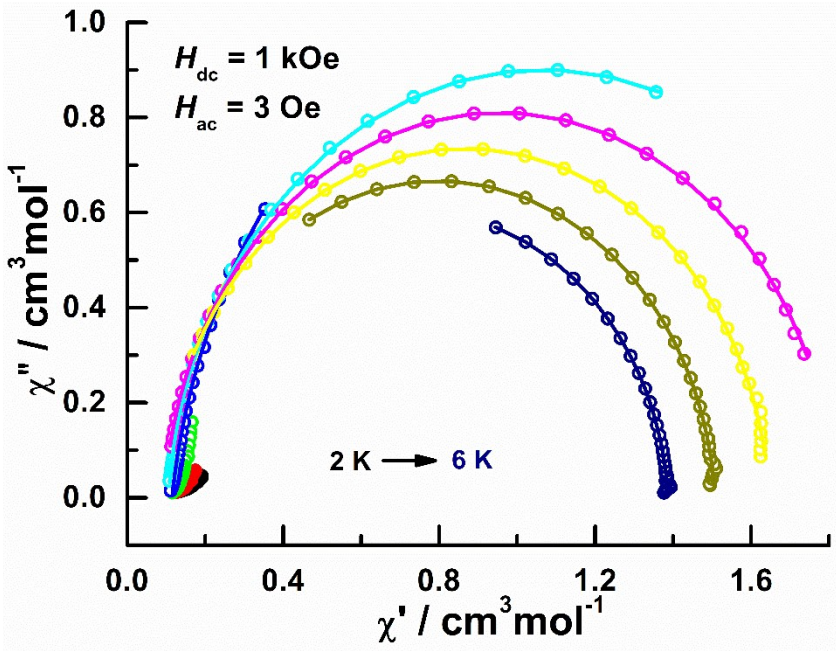

Fig. S36. The Cole−Cole plots in the range of 2−6 K (0.5 K as a step) for **5** under a 1 kOe dc field. The solid lines are the least-square fitting of the data to a distribution of single relaxation processes with the generalized Debye model.

Table S14 Relaxation parameters from the best fitting of the Cole−Cole diagrams in the range of 3.5−6 K by the generalized Debye model under a 1 kOe dc field for **5**.

T(K)	χ_S(cm^3 mol^{-1})	χ_T(cm^3 mol^{-1})	τ(s)	α
3.5	0.12	2.74	0.68E-2	0.077
4.0	0.11	2.03	0.11E-2	0.041
4.5	0.10	1.82	0.28E-3	0.037
5.0	0.09	1.65	0.81E-4	0.036
5.5	0.09	1.51	0.28E-4	0.040
6.0	0.10	1.39	0.11E-4	0.044

5. Ab initio calculations

Complexes **2**−**5** are all one-dimensional chain including a lot of Dy^{III} or Er^{III} ions, but there is one type of Dy^{III} or Er^{III} fragment for each of them. Complete-active-space self-consistent field (CASSCF) calculations on individual Dy^{III} or Er^{III} fragments (see Fig. S37−S38 for the calculated model structures of complexes **2**−**5**) on the basis of single-crystal X-ray determined geometry have been carried out with MOLCAS 8.2 program package.[5] During the calculation for **2**−**5**, the influence of distant Dy^{III} or Er^{III} ions were taken into account by the closed-shell La^{III} *ab initio* embedding model potentials (AIMP; La.ECP.deGraaf.0s.0s.0e-La-(LaMnO3.). Besides, for complexes **2** and **4**, Fe^{III} ions are all replaced with Zn^{II} ions.

The basis sets for all atoms are atomic natural orbitals from the MOLCAS ANO-RCC library: ANO-RCC-VTZP for Dy^{III} or Er^{III} ion; VTZ for close O and N; VDZ for distant atoms. The calculations employed the second order Douglas-Kroll-Hess Hamiltonian, where scalar relativistic contractions were taken into account in the basis set and the spin-orbit couplings were handled separately in the restricted active space state interaction (RASSI-SO) procedure. For the fragment of an individual Dy^{III} or Er^{III} ion, active electrons in 7 active orbitals include all *f* electrons (CAS(9 in 7) for Dy^{III} fragments and CAS(11 in 7) for Er^{III} fragments) in the CASSCF calculation. To exclude all the doubts, we calculated all the roots in the active space. We have mixed the maximum number of spin-free states which was possible with our hardware (all from 21 sextets, 128 from 224 quadruplets, 130 from 490 doublets for Dy^{III} fragments; all from 35 quadruplets, all from 112 doublets for Er^{III} fragments). SINGLE_ANISO[6−8] program was used to obtain the energy levels, $\boldsymbol{g}$ tensors, predominant m_J values, magnetic axes, *etc.,* based on the above CASSCF/RASSI-SO calculations.

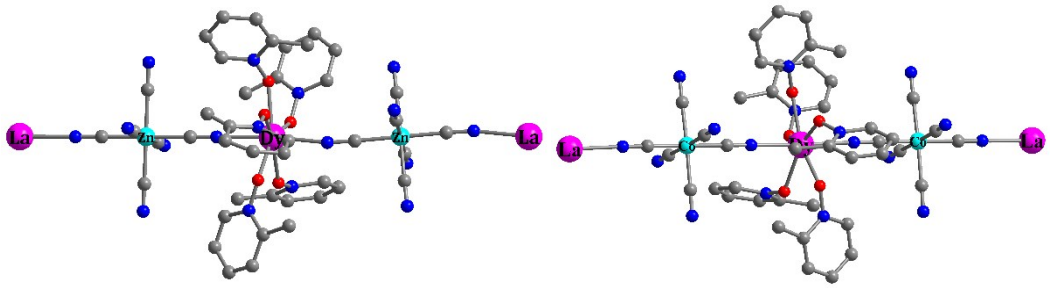

(a) (b)

Fig. S37. Calculated model structures of individual Dy^{III} fragments in complexes (a) **2** and (b) **3**; H atoms are omitted.

Table S15. Calculated energy levels (cm^{-1}), $\boldsymbol{g}$ (g_x, g_y, g_z) tensors and predominant m_J values of the lowest eight Kramers doublets (KDs) of individual Dy^{III} fragments for complexes **2** and **3** using CASSCF/RASSI-SO with MOLCAS 8.2.

KDs	**2**				**3**			
	E/cm^{-1}	$\boldsymbol{g}$		m_J	E/cm^{-1}	$\boldsymbol{g}$		m_J
1	0.0	g_x	1.446	±15/2	0.0	g_x	0.815	±15/2
		g_y	2.977			g_y	3.284	
		g_z	14.472			g_z	16.882	
2	4.9	g_x	0.657	±11/2	78.2	g_x	3.338	±13/2
		g_y	1.438			g_y	4.388	
		g_z	16.319			g_z	8.972	
3	69.4	g_x	7.308	±9/2	174.8	g_x	6.890	±3/2
		g_y	5.784			g_y	4.220	
		g_z	3.482			g_z	1.355	
4	134.1	g_x	1.352	±7/2	254.4	g_x	0.982	±11/2
		g_y	2.705			g_y	1.955	
		g_z	14.008			g_z	16.504	
5	153.5	g_x	0.386	±1/2	262.1	g_x	0.239	±7/2
		g_y	1.081			g_y	2.262	
		g_z	8.504			g_z	14.126	
6	232.7	g_x	0.776	±13/2	379.4	g_x	0.030	±5/2
		g_y	1.624			g_y	0.542	
		g_z	15.641			g_z	15.906	
7	265.8	g_x	0.634	±5/2	401.9	g_x	0.201	±9/2
		g_y	0.846			g_y	0.959	
		g_z	16.844			g_z	14.741	
8	365.6	g_x	0.072	±3/2	414.4	g_x	0.004	±1/2
		g_y	0.128			g_y	0.476	
		g_z	18.883			g_z	17.107	

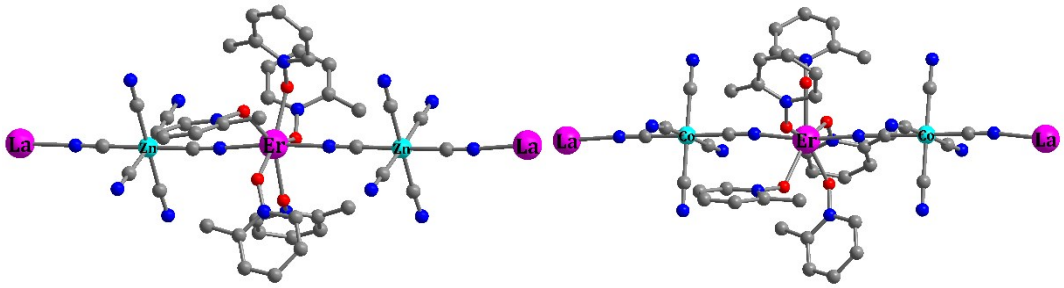

(a) (b)

Fig. S38. Calculated model structures of individual Er^{III} fragments in complexes (a) **4** and (b) **5**; H atoms are omitted.

Table S16. Calculated energy levels (cm^{-1}), $\boldsymbol{g}$ (g_x, g_y, g_z) tensors and predominant m_J values of the lowest eight KDs of individual Er^{III} fragments for complexes **4** and **5** using CASSCF/RASSI-SO with MOLCAS 8.2.

KDs	**4**				**5**			
	E/cm^{-1}	$\boldsymbol{g}$		m_J	E/cm^{-1}	$\boldsymbol{g}$		m_J
1	0.0	g_x	0.459	±13/2	0.0	g_x	0.195	±15/2
		g_y	0.968			g_y	0.246	
		g_z	15.806			g_z	15.575	
2	8.3	g_x	0.187	±9/2	29.9	g_x	0.020	±11/2
		g_y	1.416			g_y	0.392	
		g_z	14.077			g_z	12.988	
3	55.8	g_x	4.639	±7/2	102.2	g_x	2.183	±9/2
		g_y	4.786			g_y	2.575	
		g_z	8.083			g_z	9.206	
4	82.0	g_x	1.141	±5/2	142.1	g_x	2.714	±5/2
		g_y	2.550			g_y	6.041	
		g_z	12.875			g_z	10.610	
5	171.3	g_x	0.433	±1/2	234.3	g_x	0.176	±3/2
		g_y	1.394			g_y	1.774	
		g_z	15.119			g_z	14.389	
6	192.9	g_x	0.211	±11/2	244.8	g_x	0.646	±7/2
		g_y	0.916			g_y	1.361	
		g_z	16.209			g_z	13.537	
7	216.8	g_x	0.443	±3/2	267.6	g_x	0.228	±13/2
		g_y	1.145			g_y	1.269	
		g_z	16.516			g_z	15.315	
8	321.3	g_x	0.015	±15/2	289.7	g_x	0.342	±1/2
		g_y	0.025			g_y	0.729	
		g_z	17.743			g_z	16.760	

Table S17. The included angles (degree) between the magnetic axes of the ground and excited KDs for complexes **2**−**5**.

Complex	KDs	θ/°
2	1	-
	2	61.0
	3	81.8
	4	62.6
	5	77.1
	6	36.0
	7	74.1
	8	78.0
3	1	-
	2	5.2
	3	37.5
	4	75.3
	5	78.6
	6	85.2
	7	75.8
	8	89.2
4	1	-
	2	45.9
	3	22.7
	4	75.7
	5	87.6
	6	51.2
	7	80.9
	8	24.3
5	1	-
	2	13.2
	3	3.9
	4	84.3
	5	80.2
	6	56.6
	7	5.6
	8	81.1

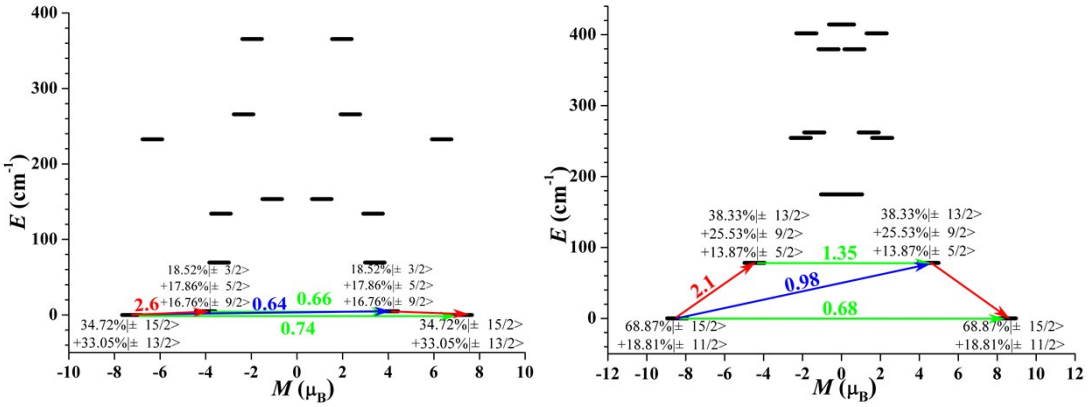

Fig. S39. Magnetization blocking barriers of individual Dy^{III} fragments in complexes **2** (left) and **3** (right). The thick black lines represent the KDs of the individual Dy^{III} fragments as a function of their magnetic moment along the magnetic axis. The green lines correspond to diagonal matrix element of the transversal magnetic moment; the blue line represent Orbach relaxation processes. The path shown by the red arrows represents the most probable path for magnetic relaxation in the corresponding compounds. The numbers at each arrow stand for the mean absolute value of the corresponding matrix element of transition magnetic moment.

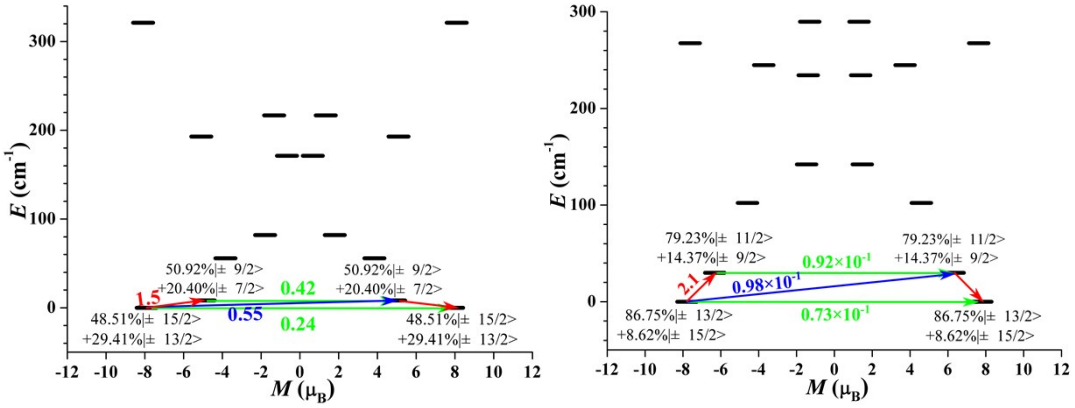

Fig. S40. Magnetization blocking barriers of individual Er^{III} fragments in complexes **4** (left) and **5** (right). The thick black lines represent the KDs of the individual Er^{III} fragments as a function of their magnetic moment along the magnetic axis. The green lines correspond to diagonal matrix element of the transversal magnetic moment; the blue line represent Orbach relaxation processes. The path shown by the red arrows represents the most probable path for magnetic relaxation in the corresponding compounds. The numbers at each arrow stand for the mean absolute value of the corresponding matrix element of transition magnetic moment.

Table S18. In wave functions with definite projection of the total moment $|m_J>$ for the lowest two KDs of the Dy^{III} or Er^{III} fragments for complexes **2**−**5**.

	E/cm^{-1}	**wave functions**
2	0.0	34.72%|±15/2>+33.05%|±13/2>
	4.9	18.52%|±3/2>+17.86%|±5/2>+16.76%|±9/2>+15.09%|±7/2>+12.83%|±1/2>
3	0.0	68.87%|±15/2>+18.81%|±11/2>
	78.2	38.33%|±13/2>+25.53%|±9/2>+13.87%|±5/2>
4	0.0	48.51%|±15/2>+29.41%|±13/2>+19.32%|±11/2>
	8.3	50.92%|±9/2>+20.40%|±7/2>
5	0.0	86.75%|±13/2>+8.62%|±15/2>
	29.9	79.23%|±11/2>+14.37%|±9/2>

6. References

1 G. M. Sheldrick, *SADABS*, *Program for Siemens area detector absorption correction*, University of Göttingen, 1996.

2 O. V. Dolomanov, L. J. Bourhis, R. J. Gildea, J. A. K. Howard and H. J. Puschmann, *Appl. Crystallogr*., 2009, **42**, 339−341.

3 (*a*) G. M. Sheldrick, *SHELXS97*, *Program for the solution of crystal structures*, University of Göttingen, Germany, 1997; (*b*) G. M. Sheldrick, *Acta Crystallogr*., *Sect. A: Fundam*. *Crystallogr*., 2008, **A64**, 112−122; (*c*) T. Shiga, M. Ohba and H. Okawa, *Inorg*. *Chem*. *Commun*., 2003, **6**, 15−18; (*d*) S. Akine, T. Matsumoto, T. Taniguchi and T. Nabeshima, *Inorg. Chem.*, 2005, **44**, 3270−3274.

4 O. Kahn, *Molecular Magnetism*, Wiley-VCH, New York, 1993.

5 F. Aquilante, J. Autschbach, R. K. Carlson, L. F. Chibotaru, M. G. Delcey, L. De Vico, I. Fdez Galvan, N. Ferre, L. M. Frutos, L. Gagliardi, M. Garavelli, A. Giussani, C. E. Hoyer, G. Li Manni, H. Lischka, D. Ma, P. A. Malmqvist, T. Muller, A. Nenov, M. Olivucci, T. B. Pedersen, D. Peng, F. Plasser, B. Pritchard, M. Reiher, I. Rivalta, I. Schapiro, J. Segarra-Marti, M. Stenrup, D. G. Truhlar, L. Ungur, A. Valentini, S. Vancoillie, V. Veryazov, V. P. Vysotskiy, O. Weingart, F. Zapata and R. Lindh, *J. Comput. Chem.*, 2016, **37**, 506−541.

6 L. Ungur and L. F. Chibotaru, *Chem. Eur. J.*, 2017, **23**, 3708−3718.

7 L. F. Chibotaru, L. Ungur, C. Aronica, H. Elmoll, G. Pilet and D. Luneau. *J. Am. Chem. Soc.*, 2008, **130**, 12445−12455.

8 L. Ungur, W. Van den Heuvel and L. F. Chibotaru, *New J. Chem.*, 2009, **33**, 1224−1230.